AD-A191 485 ROLE OF CRACKS IN THE CREEP OF STRUCTURAL POLYCRYSTALLINE CERAMICS..(U) VIRGINIA POLYTECHNIC INST AND STATE UNIV BLACKSBURG DEPT OF M.. 1/2

UNCLASSIFIED D P HASSELMAN ET AL. 15 JAN 88 F/G 11/2 NL

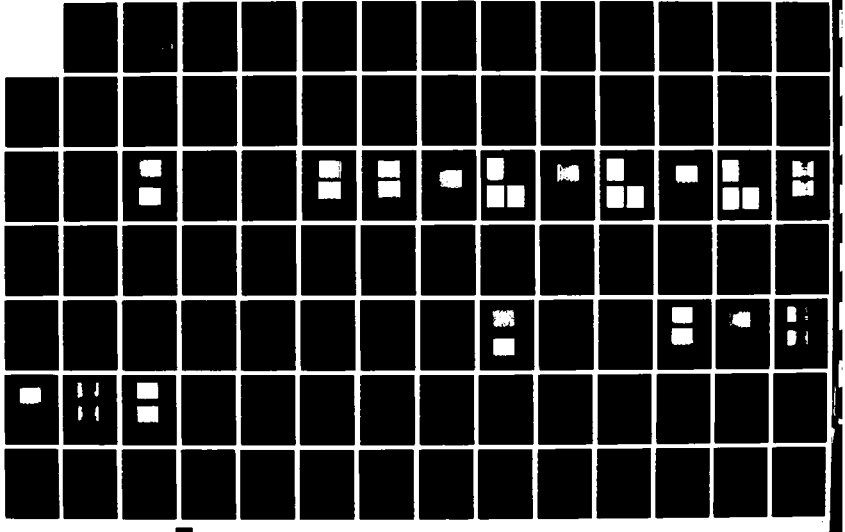

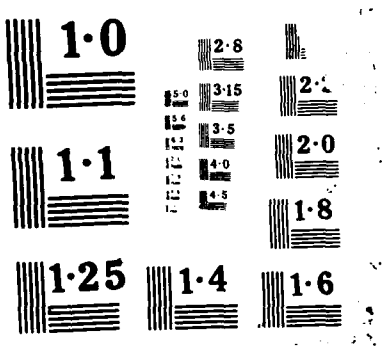
1·0
1·1
1·25
1·4
1·6
2·8
3·15
3·5
4·0
4·5
5·0
2·0
1·8

ARO 21710.7-MS

(2)

ROLE OF CRACKS IN THE CREEP

of

STRUCTURAL POLYCRYSTALLINE CERAMICS

by

D.P.H. HASSELMAN, K.Y. DONALDSON, A. VENKATESWARAN

January 15, 1988

U.S. ARMY RESEARCH OFFICE

CONTRACT: DAAG 29-85-K-0106

DEPARTMENT OF MATERIALS ENGINEERING

VIRGINIA POLYTECHNIC INSTITUTE

BLACKSBURG, VIRGINIA 24061

APPROVED FOR PUBLIC RELEASE

DISTRIBUTION UNLIMITED

REPORT DOCUMENTATION PAGE

1a. REPORT SECURITY CLASSIFICATION: Unclassified	1b. RESTRICTIVE MARKINGS
2a. SECURITY CLASSIFICATION AUTHORITY	3. DISTRIBUTION/AVAILABILITY OF REPORT: Approved for public release; distribution unlimited.
2b. DECLASSIFICATION/DOWNGRADING SCHEDULE	
4. PERFORMING ORGANIZATION REPORT NUMBER(S)	5. MONITORING ORGANIZATION REPORT NUMBER(S)
6a. NAME OF PERFORMING ORGANIZATION: Virginia Polytechnic Institute; 6b. OFFICE SYMBOL (If applicable)	7a. NAME OF MONITORING ORGANIZATION: U. S. Army Research Office
6c. ADDRESS (City, State, and ZIP Code): Blacksburg, Virginia 24061	7b. ADDRESS (City, State, and ZIP Code): P. O. Box 12211, Research Triangle Park, NC 27709-2211
8a. NAME OF FUNDING/SPONSORING ORGANIZATION: U. S. Army Research Office; 8b. OFFICE SYMBOL (If applicable)	9. PROCUREMENT INSTRUMENT IDENTIFICATION NUMBER
8c. ADDRESS (City, State, and ZIP Code): P. O. Box 12211, Research Triangle Park, NC 27709-2211	10. SOURCE OF FUNDING NUMBERS: PROGRAM ELEMENT NO. / PROJECT NO. / TASK NO. / WORK UNIT ACCESSION NO

11 TITLE (Include Security Classification): Role of Cracks in the Creep Deformation of Structural Polycrystalline Ceramics (Unclassified)

12 PERSONAL AUTHOR(S): Hasselman, D.P.H., Donaldson, Kimberly Y., Venkateswaran, Anuradha

13a. TYPE OF REPORT	13b. TIME COVERED	14. DATE OF REPORT (Year, Month, Day)	15. PAGE COUNT
Final	FROM 4/15/85 TO 9/30/87	January 15, 1988	

16. SUPPLEMENTARY NOTATION: The view, opinions and/or findings contained in this report are those of the author(s) and should not be construed as an official Department of the Army position, policy, or decision, unless so designated by other documentation.

17 COSATI CODES		
FIELD	GROUP	SUB-GROUP

18. SUBJECT TERMS (Continue on reverse if necessary and identify by block number): Alumina, elastic creep by crack growth, crack-enhanced creep, strain-rate sensitivity, cavitation, decrease in Young's modulus by crack growth, strain-softening

19 ABSTRACT (Continue on reverse if necessary and identify by block number)

A combined experimental and theoretical study was initiated to establish the validity of the concepts of elastic creep by crack growth and crack-enhanced creep and their role in the non-linear deformation and fracture behavior of polycrystalline ceramics at elevated temperatures. Elastic creep by crack growth results from the associated time-dependent decrease in Young's modulus manifested by the effect of "strain-softening" under displacement-controlled loading. Crack-enhanced creep represents an acceleration in creep-rate, due to the change in local stress distribution resulting from the presence of the cracks.

An electronic grade fine-grained alumina and a coarse-grained translucent alumina were selected for this study. Specimens in the form of circular rods were deformed in 4-point bending over a range of strain-rates under displacement

20 DISTRIBUTION/AVAILABILITY OF ABSTRACT: ☐ UNCLASSIFIED/UNLIMITED ☐ SAME AS RPT. ☐ DTIC USERS	21. ABSTRACT SECURITY CLASSIFICATION: Unclassified
22a. NAME OF RESPONSIBLE INDIVIDUAL	22b. TELEPHONE (Include Area Code) / 22c. OFFICE SYMBOL

controlled loading and over a range of temperatures at which considerable non-linear deformation prior to fracture could be observed. Both materials exhibited strain-rate dependent multiple-crack formation which was most pronounced at the intermediate values of strain rate. No crack formation was observed at the lowest strain rates, where the imposed strains could be accommodated by diffusional or other mechanisms of creep at stress levels too low for the nucleation and growth of cracks. At the highest strain rates fracture occurred at a single macrocrack due to the insufficient time for the nucleation and growth of additional cracks.

Over the intermediate to high strain rates the fine-grained alumina exhibited an unusually high strain-rate sensitivity of the failure stress. Specimens deformed to approximately 75 to 80% of the failure strain exhibited a strain-rate dependent effective Young's modulus which was decreased by as much as a factor of two from the value for the as-received specimens. A parallel theoretical analysis confirmed that the observed high strain-rate sensitivity in part could be attributed to the strain-rate dependent multiple crack-growth and associated strain-softening effect, in direct support of the concept of elastic creep.

The coarse-grained alumina deformed to about 80% of the failure strain exhibited a decrease in effective Young's modulus due to crack formation of as much as a factor of five. A parallel theoretical analysis of the stress-strain behavior confirmed that the time-dependent elastic strain contributed significantly to the observed non-linearity and total creep deformation, again in support of the concept of elastic creep.

Further details can be obtained from the pre-prints of three technical papers [1, 2, 3] based on the results of this program so far and which constitute the body of this report.

A renewal proposal was submitted for continuation of this research program.

Technical papers.

1. K.Y. Donaldson, A. Venkateswaran, D.P.H. Hasselman, "Role of Strain-Softening by Crack Formation in the Non-Linear Stress-Strain Behavior of a Polycrystalline Alumina at High Temperature, Proc. Conf. on Fractography of Glasses and Ceramics. American Ceramic Society (in press).

2. D.P.H. Hasselman, A. Venkateswaran, K.Y. Donaldson, "Contribution of Damage by Multiple Crack Growth to the Strain-Rate Sensitivity of a Polycrystalline Alumina at Elevated Temperature," J. Mat. Sc. (in review).

3. A. Venkateswaran, K.Y. Donaldson, D.P.H. Hasselman, "Role of Intergranular Damage-Induced Decrease in Young's Modulus in the Non-Linear Deformation and Fracture of an Alumina at Elevated Temperatures." J. Am. Ceram. Soc. (in press).

Role of Strain-Softening by Crack Formation in the Non-Linear Stress-Strain Behavior of a Polycrystalline Alumina at High Temperature

by

K. Y. Donaldson, A. Venkateswaran, D. P. H. Hasselman

Department of Materials Engineering

Virginia Polytechnic Institute and State University

Blacksburg, VA 24061

Role of Strain-Softening by Crack Formation in the Non-Linear Stress-Strain Behavior of a Polycrystalline Alumina at High Temperature.

K. Y. Donaldson, A. Venkateswaran, D. P. H. Hasselman
Department of Materials Engineering
Virginia Polytechnic Institute and State University
Blacksburg, VA 24061

ABSTRACT

A study was conducted of the role of crack formation in the non-linear stress-strain behavior of a fine-grained polycrystalline aluminum oxide at high temperature under conditions of displacement-rate-controlled mechanical loading.

The observed deformation behavior could be divided into three regimes. At the lowest values of deformation rate the load levelled off to a constant value without crack formation, consistent with deformation by diffusional creep. Over a range of intermediate values of deformation considerable non-linear deformation took place, manifested by a decrease in stress with increasing strain as the result of strain-softening due to the formation and growth of cracks. At the highest rates of displacement, specimen fracture occurred by the formation of a single crack without significant non-linear deformation and without the formation of additional cracks.

These results are discussed in terms of the general mechanisms and kinetics of the deformation of non-ductile solids.

INTRODUCTION

Many structural materials can exhibit non-linear stress-strain characteristics. Under conditions of constant rate of loading such non-linear behavior generally is referred to as plastic or viscous flow [1,2]. Under conditions of time-invariant stress, non-linear stress-strain response is referred to as creep [1,2]. Extensive research has shown that for polycrystalline solids the rate of creep deformation depends on the magnitude of stress, temperature and microstructural variables such as grain size and pore content as well as the available mechanisms for non-linear deformation. These mechanisms include dislocation glide and climb [3,4] as well as diffusional creep by volume or grain boundary diffusion [5,6,7]. Amorphous materials such as glasses can deform by viscous flow [8]. Polycrystalline structural ceramics, unless very close to the melting point, generally deform by volume or grain-boundary diffusional creep or by viscous flow of an amorphous grain boundary phase [9,10].

The formation and growth of microcracks also is increasingly recognized as a major contributor to the non-linear deformation of brittle structural materials. The basic reason for this effect is that due to the redistribution of the stress, the presence of the cracks results in a reduction in the effective elastic moduli [11,12,13]. For this reason, the formation and growth of microcracks results in a time-dependent increase in elastic strain. For the non-linear deformation of concrete and rock under conditions of constant strain-rate loading, this effect is referred to as strain-softening [14-18]. Under constant load the time-dependent elastic strain results in elastic or compliance creep [19]. The presence of stationary cracks results in an increase in the creep rate over the rate of

creep for the crack-free solid. This mechanism, referred to as "crack-enhanced" creep [20], was originally formulated for Griffith cracks by Weertman [21] and extended to penny-shaped cracks by Hasselman and Venkateswaran [20].

In recent years, the deformational characteristics of brittle materials have been analyzed in terms of the criterion of stress-induced damage, a concept applied to such materials as concrete, rock, ice, composites and ceramics [22-35].

The formation of microcracks in brittle structural ceramics is well recognized. Such microcracks can form as the result of a number of effects. In single-phase polycrystalline ceramics, thermal expansion anisotropy of the individual grains can result in internal stresses of sufficiently high magnitude to result in spontaneous microcrack formation [36]. The presence of these microcracks can have a major effect on Young's modulus [37], fracture energy [37], thermal insulating ability [38] and thermal shock resistance [39-41]. Stress-induced microcracking can cause a significant increase in fracture toughness [42]. Similar effects can occur in brittle matrix composites with mismatches in the coefficients of thermal expansion of the individual components. Extensive experimental work has also shown that the presence of microcracks can have a profound effect on the mechanical response of geological materials at ambient temperatures [43-49].

At elevated temperatures, microcracking in polycrystalline structural ceramics under mechanical load can result from grain-boundary sliding [50] and cavitation [51-53]. Viscous deformation of a glassy phase also can lead to grain-boundary separation and associated crack formation. Microscopy of ceramic specimens following creep deformation has shown that microcrack formation under conditions of tensile stress occurs at grain

boundary facets oriented perpendicular to the stress [54]. In contrast, under compressive load grain boundary separation occurs along grain boundaries oriented parallel to the applied stress [55].

It is being recognized that microcrack formation can have a significant effect on the creep deformation and related mechanical behavior of structural ceramics. The creep rate and failure time due to subcritical crack growth are closely related [56-61]. Due to the stress dependence of microcrack formation, polycrystalline ceramics can exhibit apparent non-linear creep as the result of the mechanism of crack-enhanced creep even if the underlying creep mechanism exhibits a linear relationship between stress and creep rate [20]. For the same reason, an anomalous grain-size dependence of creep rate is expected [20], in agreement with observation [62]. The concept of crack-enhanced creep was used to effectively clarify an apparent discrepancy between values for the diffusion coefficient for aluminum oxide measured directly and those inferred from creep data [63]. Intergranular cracking has also been shown to be the dominant mechanism in the relaxation of residual stresses in polycrystalline aluminum oxide at temperatures (~850 ^{o}C) far too low for diffusional creep processes to make a significant contribution [64]. It is also being recognized that damage formation by microcracking or other mechanisms in the tensile stress zone of bend specimens introduces an additional complicating factor in the interpretation of creep data obtained in bending [63, 65].

Experimental data for the stress dependence of the creep behavior of polycrystalline structural ceramics appear to be inconsistent. Using the method of constant displacement rate loading, Folweiler [54] found that the creep rate of polycrystalline aluminum oxide depended linearly on stress, as expected for diffusional creep by the Nabarro-Herring [5,6] or Coble [7]

mechanisms. However, a photomicrograph of a specimen surface following creep deformation showed extensive intergranular crack formation, which could have led to an apparent non-linear creep behavior. A number of other investigations showed that polycrystalline aluminum oxide exhibited non-linear creep behavior [66-68].

Non-linear creep response was also observed for hot-pressed silicon nitride by Arons and Tien [69], who concluded that cavitation at least in part was a contributing factor. In terms of the results of the present study to be related shortly, Fett and Munz [70] found that hot-pressed silicon nitride subjected to creep by dynamic bending also showed highly non-linear creep response. However, no microstructural evidence was presented as to whether microcracking or cavitation played a role. In a related study also of interest to the present investigation, Fett and Munz [71] concluded that crack growth parameters at high temperature inferred from the loading rate sensitivity of the tensile strength can be affected by creep deformation.

The present paper is a first report of a study of the role of crack formation and associated effects on the stress-strain, creep and failure characteristics of polycrystalline structural ceramics. Specifically, observations will be reported of the effect of strain-softening by crack formation on the strain-rate sensitivity of the failure stress. In terms of the theme of the conference, the present report will emphasize the fractographic aspects of the effect of strain-softening by crack formation. A theoretical analysis is intended to be the subject of a future report.

EXPERIMENTAL

A. Material

The test material chosen for this study consisted of a substrate-quality, relatively fine-grained polycrystalline aluminum oxide known as AlSiMag 838, made by the 3M Corporation. The scanning electron micrograph of a room temperature fracture surface shown in fig. 1 indicates that this material is nearly fully dense with an average grain size of ~5 μm and an occasional grain as large as 20 μm. For purpose of future comparison, fig. 2 shows a scanning electron micrograph of a polished section through an annealed undeformed specimen, which indicates the presence of an occasional pore without any preferred pore orientation.

The test samples were in the form of circular rods with a length of ~50 mm and a diameter of ~4.8 mm. Prior to testing all samples were annealed at about 1000 ^{o}C for 6-7 hr to minimize the effect of residual stresses, if any.

B. Test procedures

The specimens were tested in 4-point bending with inner and outer spans of 10 and 40 mm, resp. The specimen holder consisted of silicon carbide, the load to the specimens being transferred by silicon carbide pins which were permitted to rotate freely in order to keep extraneous stresses to a minimum. Testing was done in an argon atmosphere within an environmental chamber resistively heated with tungsten mesh heating elements. The environmental chamber was contained within the load-frame of an electro-hydraulic closed-loop mechanical tester made by the MTS Corporation. The

displacement of the actuator and the resulting load were transferred via graphite push-rods and water-cooled bellows to the specimen and load cell, resp. The displacement of the actuator was measured using a displacement gauge, held against the actuator outside of the environmental chamber. This gauge, with a range of ~4 mm, permitted measurement of the displacement to within a few μm. By making a separate measurement of the elastic displacement of the total load train without specimen, the displacement of the loading points of the specimens could be obtained by the appropriate subtraction. For the test material and specimen size of this study, the elastic displacement of the specimen and load train were approximately equal in value. The load as a function of time was recorded with an x-y recorder for most values of displacement rate and an oscilloscope at the highest value of displacement rate.

The specimens were loaded over a range of values of constant displacement rates and temperatures ranging from room temperature to as high as 1450 ^{o}C. The displacement-load data were converted to strain and stress using the theory for bending of homogeneous beams.

Following testing, the specimen external and fracture surfaces (if broken), were examined by scanning electron microscopy. The specimens were also sectioned by a slow-speed diamond saw and then diamond-polished to provide a crossection of the specimen interior ranging from the line of maximum tensile stress to the maximum compressive stress.

RESULTS AND DISCUSSION

Fig. 3 shows the stress-strain behavior of the alumina specimens for four different rates of displacement and temperatures ranging from room temperature to as high as 1450 ^{o}C. The stress-strain behavior at room temperature and at 1000 ^{o}C is linear, indicative of totally elastic deformation and the absence of any non-linear mechanical response. At temperatures above 1300 ^{o}C, however, considerable deviation from linearity can be noted, with the amount of non-linear strain prior to fracture increasing with increasing temperature and decreasing with increasing displacement rate. At the lowest value of displacement rate and highest values of temperature, the specimen deformed at a sufficiently high rate that the fracture stress was not exceeded over the total range of non-linear deformation.

In terms of the objectives of this study, two observations are noteworthy. Firstly, the stress-strain curves obtained at the highest values of temperatures and lowest values of displacement rate indicate that the stress rises to a value which remains constant over the total range of non-linear deformation. For constant rate of displacement, this behavior is consistent with any mechanism of creep, whether linear or non-linear, by which the specimen deforms by a homogeneous mechanism, i. e., creep by grain boundary or volume diffusion or creep by dislocation glide or climb, for which a work-hardening mechanism is absent.

Secondly, a number of the stress-strain curves at strains immediately prior to fracture show a decrease in stress with increasing strain. Such stress-strain behavior is incompatible with the conventional mechanisms of creep and is indicative of a mechanism of non-linear deformation which leads to the effect of "strain- softening". The existence of an upper and

lower yield point such as is found in some metals would constitute one such mechanism. This mechanism, however, is not expected to operate in structural ceramics such as alumina. For this reason, an alternative mechanism must be found.

In order to establish a basis for such a mechanism, fig. 4 shows the values of maximum load during creep or fracture reached during deformation as a function of displacement for the four temperatures used in this study. Usually, these data represent the load at failure with the exception of the data obtained at the highest temperature and lowest value of displacement rate, which represent the maximum load reached during deformation in the absence of failure. Fig. 4 shows a number of effects. The load at failure (or creep load) rises with increasing displacement rate at all values of temperature. This is in accordance with the generally expected dependence of deformation or fracture on loading-rate.

At 1300 ^{o}C, the dependence of the load at failure on displacement rate shows a downward curvature over the total range of displacement rate. Such dependence is in general agreement with the behavior predicted by Fett and Munz [70, 71], the loads at failure being controlled by creep deformation at the lowest rate of displacement and by sub-critical crack growth of a single flaw at the highest rates of displacement.

In contrast, the dependence of load at fracture on displacement rate at 1350, 1400 and 1450 ^{o}C shown in figs. 4b, 4c and 4d, resp., indicates significantly different behavior. These data appear to indicate the existence of three different regimes. In the first regime at the lowest values of displacement rates, the load rises with increasing displacement rate. Such behavior is in accordance with deformation and eventual fracture by homogeneous creep, in agreement with the theory of Fett and Munz [70, 71]. In the intermediate regime, the load at fracture shows a

distinct upward curvature with increasing displacement rate and corresponding rapid increase in strain-rate sensitivity, i. e., the slope of the load vs. displacement curve. The maximum magnitude of the strain-rate sensitivity is far greater than could be accounted for by the strain-rate sensitivity controlled by sub-critical crack growth alone [71, 72]. Clearly, in the intermediate regime of displacement rate some mechanism other than sub-critical crack growth must make the primary contribution.

In the third regime, at the very highest values of displacement rate the load again levels off to become nearly independent of displacement rate. For experimental reasons, the number of data in this regime are insufficient to establish a quantitatively significant dependence of load on displacement rate, in view of the well-known scatter of strength values for brittle materials such as the aluminum oxide of this study. However, it is thought that this third regime corresponds to failure by sub-critical crack growth unaffected by creep deformation, again in accordance with the theory of Fett and Munz [70, 71].

An explanation for the existence of the three regimes for the dependence of failure load on displacement rate was established by microscopy of the specimens following deformation and fracture.

Figs. 5a and 5b show SEM-micrographs of polished sections near the line of maximum tensile stress (at or near the right-hand side of the figures) of specimens deformed at ~1300 ^{o}C at displacement rates of 0.005 and 0.05 cm/min. The specimen deformed at 0.005 cm/min clearly indicates evidence for crack formation. As indicated by their dimensions relative to the scale of the microstructure as well as their preferred path of propagation, crack formation in the alumina tested under the conditions of this study appears to occur by the growth of microcracks along the grain boundaries

rather than by the formation of isolated intergranular cracks of the order of the grain size, such as those observed by Folweiler and others [54, 55]. No crack formation could be detected in the regions of the specimen of fig. 5a subjected to compressive loading.

At 1300 ^{o}C no crack formation was observed in specimens deformed at displacement rates >0.005 cm/min as indicated by the SEM-micrograph of fig. 5b of a polished section of a specimen deformed at a displacement rate of 0.05 cm/min.

The formation of cracks is also evident on the tensile specimen surface, as shown in fig. 6 for the two specimens of fig. 5. Fig. 6a clearly indicates the intergranular nature of crack propagation at the displacement rate of 0.005 cm/min. No crack formation, other than the crack at the site of fracture, could be detected in the specimen deformed at 0.05 cm/min, as shown by the SEM-micrograph of fig. 6b.

Further evidence of the primarily intergranular nature of crack propagation is shown by the SEM-fractograph of fig. 7 near the site of fracture of the specimen of fig. 5b and 6b deformed at ~1300 ^{o}C at 0.05 cm/min. Such intergranular fracture generally was found at all testing temperatures of this study >1300 ^{o}C.

Figs. 8a, b and c show polished sections of specimens deformed at 1350 ^{o}C at displacement rates of 0.005, 0.5 and 5 cm/min, resp., with the right-hand side of the figure at or near the line of maximum tensile stress. It should be noted that the specimen deformed at the intermediate value of displacement rate of 0.5 cm/min shows evidence for intergranular cracking perpendicular to the tensile stress, whereas such crack formation is absent in the specimens deformed at the displacement rates of 0.005 and 5 cm/min.

Fig. 9 shows a scanning electron-micrograph of the tensile fracture surface and the tensile specimen surface immediately adjacent to the plane of fracture of the same specimen as for fig. 8b, deformed at 1350 ^{o}C at 0.5 cm/min. The specimen surface gives evidence for crack development at positions adjacent to the plane of fracture. One such crack appears to have been nucleated at a large grain.

Figs. 10a, b and c show polished sections of specimens deformed at ~1400 ^{o}C at displacement rates of 0.005, 0.5 and 5 cm/min, resp. Again, as for the specimen deformed at 1350 ^{o}C, crack formation was found only at the intermediate rate of displacement of 0.5 cm/min, and was absent at the lower and higher values of displacement rate of 0.005 and 5 cm/min. A surface crack in the specimen deformed at 0.5 cm/min is shown in fig. 11.

Polished sections for specimens deformed at ~1450 ^{o}C at displacement rates of 0.01, 0.5 and 10 cm/min are shown in figs. 12a, b and c, resp. As indicated by these three micrographs, crack formation occurred at the intermediate displacement rate of 0.5 cm/min, whereas no microstructural change appears to have occurred in those specimens deformed at 0.01 and 10 cm/min.

In order to indicate that crack formation occurred over a range of intermediate values of displacement rates at 1450 ^{o}C, figs. 13a and 13b show SEM- micrographs of the surfaces of specimens deformed at ~1450 ^{o}C at displacement rates of 1 and 2 cm/min, resp, which clearly indicate the presence of cracks. No crack formation could be detected in specimens subjected to displacement rates of <0.05 cm/min or >5 cm/min.

The fractographic evidence presented in figs. 5 through 13 confirms the earlier conclusion based on the data shown in fig. 4, that the dependence of fracture load on displacement rate at 1350, 1400 and 1450 ^{o}C appears to indicate the existence of three different regimes. Comparison of figs. 4b,

c and d with the electron micrographs of figs. 8 thru 13 suggests that the intermediate regime represents the range of displacement rate over which substantial sub-critical crack growth occurred. At 1300 ^{o}C, the fractographic evidence suggests the existence of only two regimes. However, it is speculated that if data had been obtained at displacement rates $<<0.005$ cm/min, some lower value of displacement rate would have been found below which no crack formation would have occurred.

Clearly, the existence of three regimes in the dependence of failure load on displacement rate must be explainable in terms of the effect of the external variables such as loading rate, temperature, etc., and internal variables such as grain size, pore content and pore size on creep, crack formation and fracture of the material of this study.

It is proposed that the three separate regimes are controlled by the following primary mechanisms.

In the first regime, which occurs at the lowest values of displacement rate, at which the load reaches a constant value without failure over the total duration of loading, deformation is controlled by diffusional creep only, the magnitude of stress reaching a value which is too low for cavitation and/or subcritical crack growth to occur.

The second regime represents intermediate values of displacement rates, at which the stress level rises to values in excess of the minimum stress required for the growth of cracks from pores or nucleated cavities. In this regime the specimen is loaded over a sufficiently long period that the extent of sub-critical crack growth of all cracks being formed is sufficient to cause a significant decrease in Young's modulus and associated decrease in load. This, in effect, represents "strain-softening", and results directly from the "damage" due to the formation of the cracks. Such strain-softening represents the primary mechanism which

controls the maximum load attained, with a secondary contribution from diffusional creep, which, in turn, is enhanced by the presence of the cracks. Because the amount of sub-critical crack growth is a function of the length of time under load, the effect of "strain-softening" is expected to decrease with increasing displacement rate, in agreement with observations.

The third regime represents rates of loading for which the time-to-failure is too short to result in significant crack formation. Under these conditions the decrease in Young's modulus is insignificant, with the failure stress controlled primarily by the sub-critical growth, if any, of the failure-initiating flaw, with diffusional creep making a secondary contribution.

Fig. 14 is a schematic representation of the existence of the three regimes for the dependence of maximum or failure load on the displacement rate. The data in the regime corresponding to the lowest displacement rates can be used to ascertain the value of the stress exponent for creep, whereas the data in the regime for the highest values of displacement rate will yield the value for the stress intensity exponent for sub-critical crack growth. The data in the regime corresponding to the intermediate values are subject to a number of variables simultaneously, such that the interpretation of data in this regime of loading-rate is expected to be quite complex.

The data obtained at 1350, 1400 and 1450 ^{o}C, shown in figs. 4b, c and d, resp, exhibit the existence of all three of the above regimes. At 1300 ^{o}C, the rate of creep deformation is too slow to result in the formation of all three regimes. With the exception of the very lowest values of displacement rates, the majority of data reflect the change in fracture stress due to sub-critical crack growth, i.e., the regime of strain-rate

sensitivity.

In view of the above discussion, it also can be concluded that the non-linear stress-strain behavior exhibited by the data of fig. 3 should be attributed to the combined effects of creep and crack formation rather than to other mechanisms for non-linear deformation such as dislocation motion and/or multiplication.

The observations and conclusions of this study should be critical to the general area of the measurement of the mechanical behavior of structural ceramics at elevated temperatures. As discussed extensively in earlier studies [20, 73], under conditions of constant stress, crack formation can lead to accelerated creep due to the combined effects of elastic and crack-enhanced creep, as well as to an anomalous stress and grain-size dependence. The shape of the creep curve also can be significantly affected by crack formation.

The interpretation of non-linear stress-strain behavior should be approached with a great deal of caution. Crack formation as affected by loading rate and temperature will have a qualitatively similar effect on non-linearity as do dislocation motion and multiplication. For instance, it is the view of these authors that the well-known observations of the non-linear stress-strain behavior of polycrystalline UO_2, reported by Canon, et al. [74], should be attributed to the mechanism of strain-softening rather than dislocation-controlled phenomena.

Crack formation and associated "strain-softening" also could have a significant effect on the data for creep behavior obtained by constant displacement rate loading, i.e., dynamic creep. Under these conditions, information on the basic underlying mechanism of creep can be obtained only by using displacement rates sufficiently low so that crack formation is avoided. If such tests are conducted at stress levels sufficiently high so

that intergranular cracking cannot be avoided, anomalous data will be observed. It is for this very reason that it appears very puzzling to the present authors that Folweiler [54], in spite of extensive intergranular cracking in the polycrystalline alumina selected for his study, nevertheless found that the creep rate depended linearly on stress. The only plausible explanation for this finding is that all of Folweiler's specimens exhibited the same relative degree of crack formation so that, in fact, the observed creep rate represented "crack-enhanced" creep. In support of this latter hypothesis is that the concept of crack-enhanced creep applied to Folweiler's data served quite successfully to explain the apparent discrepancy between diffusion coefficients inferred from the creep data and those measured directly [63].

The mechanism of strain-softening by crack formation also can have a significant effect on the data for the stress intensity factor exponent for sub-critical crack growth obtained by measurements of the strain-rate sensitivity in constant displacement rate loading. In two recent papers, Fett and Munz [70, 71] recognize that measurements of the strain-rate sensitivity at high temperatures can be affected by accompanying creep deformation. They predict the existence of two regimes of failure stress as a function of displacement rate. One regime occurs at very low displacement rates controlled by creep, and the other regime at the highest displacement rates is controlled by the sub-critical growth of the failure-initiating flaw, with a smooth transition between both regimes at intermediate displacement rates. It is critical to note that the theory of the strain-rate sensitivity of brittle materials is based on the implicit assumption that failure occurs as the result of the sub-critical growth of a single crack without any significant change in specimen compliance.

If, however, other cracks exhibit significant sub-critical growth, even if they do not contribute to the actual failure, the load at fracture can be decreased significantly by the associated effect of strain-softening whenever such tests are conducted under conditions of controlled displacement rates. Especially, if the amount of crack formation is a function of the displacement rate, as found in this study, the effect of strain-softening will cause an anomalous strain-rate sensitivity. In the presence of strain-softening, the theory of Fett and Munz needs to be modified to include the intermediate regime as suggested by the results of this study and schematically illustrated in fig. 14.

In general, it is expected that the effect of strain-softening on the mechanical behavior of structural ceramics will not be similar for different materials. It is anticipated that strain-softening will be found more often in those materials prone to intergranular cracking, i.e. those materials with large grain size and those with a low viscosity glassy grain-boundary phase.

An analysis of the effect of strain-softening by crack growth will be the subject of a future report.

Acknowledgment.

This study was supported by the Army Research Office under Contract No. DAAG 29-85-K-0106.

REFERENCES

1. G. E. Dieter, Mechanical Metallurgy, 2nd. ed., McGraw Hill Inc. (1976)
2. W. D. Kingery, H. K. Bowen and D. R. Uhlmann, Introduction to Ceramics, 2nd ed., Wiley, N. Y. (1976)
3. N. F. Mott, Conference on Creep and Fracture of Metals at High Temperatures, 0.21, H. M. Stationery Office, London (1956)
4. J. Weertman, "Dislocation Climb Theory of Steady-State Creep", Amer. Soc. of Met. Trans. 61, 681-693 (1968)
5. F. R. N. Nabarro, "Deformation of Crystals by the Motion of Single Ions, Strength of Solids", The Physical Society, London, 75 (1948)
6. C. Herring, "Diffusional Viscosity of a Polycrystalline Solid", J. Appl. Phys. 21, 437 (1950)
7. R. L. Coble, "A Model for Boundary Diffusion Controlled Creep in Polycrystalline Materials", J. Appl. Phys. 34, 1679-1684 (1964)
8. H. S. Y. Hsich, "Physical and Thermodynamic Aspects of the Glassy State and Intrinsic Non-Linear Behavior of Creep and Stress Relaxation", J. Mat. Sci. 15, 1194-1206 (1980)
9. R. Morrell and K. H. G. Ashbee, "High Temperature Creep of Lithium Zinc Silicate Glass-Ceramics", J. Mat. Sci. 8, 1253-1270 (1973)
10. R. Kossowsky, D. G. Miller and E. S. Diaz, "Tensile and Creep Strengths of Hot-Pressed Si_3N_4", J. Mat. Sci. 10, 983-997 (1975)
11. J. B. Walsh, "Effect of Cracks on the Compressibility of Rocks", J. Geophys. Res. 70 (2), 381-89 (1965)
12. R. L. Salganik, "Mechanics of Bodies with Many Cracks", Izv. Akad. Nauk. SSR, Mekh. Tverd. Tela. 8, 149-158 (1973)
13. B. Budiansky and R. J. O'Connell, "Elastic Moduli of a Cracked Solid", Int. J. Solid Struct. 12, 81-97 (1976)

14. S. K. Ghosh and M. Z. Cohn, "Non-Linear Analysis of Strain-Softening Structures", pp. 315-332 in Inelasticity and Non-Linearity in Structural Concrete, Ed. by M. Z. Cohn, University of Waterloo Press, Waterloo (1973)

15. G. Maier, A. Zavelani and J. Dotreppe, "Equilibrium Branching Due to Flexural Softening", J. Eng. Mech. Div., ASCE, 99 (EM 4) 897-901 (1973)

16. Z. P. Bazant, "Instability, Ductility, and Size-Effect in Strain-Softening Concrete", J. Eng. Mech. Div., ASCE, 102 (E 2) 331-344 (1976)

17. Z. P. Bazant and B. H. Oh, "Rock Fracture via Strain-Softening Finite Elements", J. Eng. Mech. Div., ASCE, 110 (7) 1015-1035 (1984)

18. E. P. Chen and L. M. Taylor, "Fracture of Brittle Rock Under Dynamic Loading Conditions", pp. 175-86 in Fracture Mechanics of Ceramics, Vol. 7, ed. by R. C. Bradt, A. G. Evans, D. P. H. Hasselman and F. F. Lange, Plenum Press (1986)

19. A. Venkateswaran and D. P. H. Hasselman, "Elastic Creep of Stressed Solids Due to Time-Dependent Changes in Elastic Properties", J. Mat. Sci. 16, 1627-1632 (1981)

20. D. P. H. Hasselman and A. Venkateswaran, "Role of Cracks in the Creep Deformation of Brittle Polycrystalline Ceramics", J. Mat. Sci. 18, 161-172 (1983)

21. J. Weertman, "Effect of Cracks on Creep Rate", Trans. Amer. Soc. Met. 62, 502-511 (1969)

22. D. Krajcinovic and G. U. Fonseka, "The Continuous Damage Theory of Brittle Materials, Part 1: General Theory", J. Appl. Mech. 48 (4) 809-815 (1981)

23. G. U. Fonseka and D. Krajcinovic, "The Continuous Damage Theory of Brittle Materials, Part 2: Uniaxial and Plane Response Models", J. Appl. Mech. 48 (4) 816-824 (1981)

24. D. Krajcinovic and M. A. G. Silva, "Statistical Aspects of the Continuous Damage Theory", Int. J. Solid Structures 18 (7) 551-562 (1982)

25. D. Krajcinovic, "Constitutive Equations for Damaging Materials", J. Appl. Mech. 50 (2) 355-360 (1983)

26. D. Krajcinovic, "Creep of Structures - A Continuous Damage Mechanics Approach", J. Struct. Mech. 11 (1) 1-11 (1983)

27. M. Lorrain and K. E. Loland, "Damage Theory Applied to Concrete", pp. 341-369 in Fracture Mechanics of Concrete, ed. by F. H. Whitman, Elsevier, Amsterdam (1983)

28. M. Bocek and M. Hoffmann, "The Influence of Cavitation Damage upon High Temperature Creep Under Stationary and Non-Stationary Loading Conditions, Part 1: The Model Description", J. Nucl. Mat. 125 (1) 1-6 (1984)

29. M. Bocek and M. Hoffmann, "The Influence of Cavitation Damage Upon High-Temperature Creep Under Stationary and Non-Stationary Loading Conditions, Part 2: Tensile Creep At Constant Load and Constant True Stress Resp.", J. Nucl. Mat. 125 (1) 7-18 (1984)

30. M. Bocek and M. Hoffmann, "The Influence of Cavitation Damage Upon High-Temperature Creep Under Stationary and Non-Stationary Loading Conditions, Part 3: Creep At Steady Increasing Load and True Stress", J. Nucl. Mat. 126 (3) 285-291 (1984)

31. M. Bocek and M. Hoffmann, "The Influence of Cavitation Damage Upon High-Temperature Creep Under Stationary and Non-Stationary Loading Conditions, Part 4: Cyclic Creep At Constant Amplitude and Constant True Stress Amplitude", J. Nucl. Mat. 126 (3) 292-303 (1984)

32. M. Bocek, "High Temperature Tensile Creep, Creep Damage and Failure Under Superimposed Compressional Stress", J. Nucl. Mat. 131 (1) 267-279 (1985)

33. M. P. Wnuk and R. D. Kriz, "CDM Model of Damage Accumulation in Laminated Composites", Int. J. of Fract. 28 (3) 121-138 (1985)

34. D. G. Karr, "A Damage Mechanics Model for Uniaxial Deformation of Ice", J. Energy Resources Tech. 107 (3) 363-368 (1985)

35. A. R. Rosenfield, W. H. Duckworth and D. L. Shetty, "Damage Analysis of Creep in Bending", J. Amer. Ceram. Soc. 68 (9) 483-485 (1985)

36. A. G. Evans, "Microfracture from Thermal Expansion Anisotropy - I, Single Phase Systems", Acta Metall. 26, 1845-53 (1978)

37. J. A. Kuszyk and R. C. Bradt, "Influence of Grain Size on Effects of Thermal Expansion Anisotropy in $MgTi_2O_5$", J. Amer. Ceram. Soc. 56 (8) 429-23 (1973)

38. D. P. H. Hasselman, "Effects of Cracks on Thermal Conductivity", J. Comp. Mater. 12 (10) 403-407 (1978)

39. D. P. H. Hasselman, "Unified Theory of Thermal Shock Fracture Initiation and Crack Propagation in Brittle Ceramics", J. Amer. Ceram. Soc. 52 (11) 600-04 (1969)

40. R. C. Rossi, "Thermal-Shock-Resistant Ceramic Composites", Amer. Ceram. Soc. Bull. 48 (7) 736-37 (1969)

41. D. P. H. Hasselman and J. P. Singh, "Analysis of Thermal Stress Resistance of Microcracked Brittle Ceramics", Amer. Ceram. Soc. Bull. 58 (9) 856-60 (1979)

42. Y. Fu and A. G. Evans, "Microcrack Zone Formation in Single Phase Polycrystals", Acta Metall. 30, 1619-25 (1982)

43. W. F. Brace and E. G. Bombolakis, "A Note on Brittle Crack Growth in Compression", J. Geophysical Res. 68 (12) 3709-13 (1963)

44. N. G. W. Cook and K. Hodgson, "Some Detailed Stress-Strain Curves for Rock", J. Geophysical Res. 70 (12) 2833-88 (1965)

45. W. F. Brace, B. W. Paulding, Jr. and C. Scholz, "Dilatancy in the Fracture of Crystalline Rocks", J. Geophysical Res. 71 (16) 3939-53 (1966)

46. C. H. Scholz, "Experimental Study of the Fracturing Process in Brittle Rock", J. Geophysical Res. 73 (4) 1947-54 (1968)

47. C. H. Scholz, "Mechanism of Creep in Brittle Rock", J. Geophysical Res. 73 (10) 3295-3302 (1968)

48. D. J. Holcomb, "Memory, Relaxation and Microfracturing in Dilatant Rock", J. Geophysical Res. 86 (B7) 6235-48 (1981)

49. P. L. Swanson, "A Fracture Mechanics and Non-Destructive Evaluation Investigation of the Subcritical-Fracture Process in Rock", pp. 299-318 in Fracture Mechanics of Ceramics, Vol. 8, ed. by R. C. Bradt, A. G. Evans, D. P. H. Hasselman and F. F. Lange, Plenum Press (1986)

50. A. G. Evans, "Deformation and Failure Caused by Grain Boundary Sliding and Brittle Cracking", Acta Metall. 28, 1155-64 (1980)

51. T. J. Chuang, K. I. Kagawa, J. R. Rice and L. B. Sills, "Non-Equilibrium Models for Diffusive Cavitation of Grain Interfaces", Acta Metall. 27, 265-84 (1979)

52. T. J. Chuang, "A Diffusive Crack-Growth Model for Creep Fracture", J. Amer. Ceram. Soc. 65, 93-103 (1982)

53. F. H. Vitovec, "Cavity Growth and Creep Rate Taking Into Account the Change of Net Stress", J. Mat. Sci. 7, 615-620 (1962)

54. R. C. Folweiler, "Creep Behavior of Pore-Free Polycrystalline Aluminum Oxide", J. Appl. Phys. 32 (5) 773-78 (1961)

55. J. B. Ainscough, F. Rigby, S. A. Morrow, "Effect of Oxygen Potential on the Thermal Creep of Niobia-Doped UO_2", J. Amer. Ceram. Soc. 64 (5) 315-18 (1981)

56. F. C. Monkman and N. J. Grant, "An Empirical Relationship Between Rupture Life and Minimum Creep Rate in Creep-Rupture Tests", Proc. Amer. Soc. Test. Mater. 56, 593-620 (1956)

57. F. F. Lange, "Interrelations Between Creep and Slow Crack Growth for Tensile Loading Conditions", Int. J. of Fracture 12 (5) 739-44 (1976)

58. H. E. Evans, Mechanisms of Creep Fracture, Elseviers Applied Science Publishers (1984), 319 pp.

59. B. J. Dalgleish, S. M. Johnson and A. G. Evans, "High-Temperature Failure of Polycrystalline Alumina: I, Crack Nucleation", J. Amer. Ceram. Soc. 67 (11) 741-50 (1984)

60. W. Blumenthal and A. G. Evans, "High-Temperature Failure of Polycrystalline Alumina: II, Creep Crack Growth and Blunting", J. Amer. Ceram. Soc. 67 (11) 751-59 (1984)

61. S. M. Johnson, B. J. Dalgleish and A. G. Evans, "High-Temperature Failure of Polycrystalline Alumina: III, Failure Times", J. Amer. Ceram. Soc. 67 (11) 759-63 (1984)

62. B. Burton, G. L. Reynolds, J. P. Barnes, "The Influence of Grain Size on the Creep of Uranium Dioxide", J. Mat. Sci. 8, 1690-94 (1973)

63. A. Venkateswaran and D. P. H. Hasselman, "Creep Analysis of Bend Specimens Subject to Tensile Cracking", Communications Amer. Ceram. Soc. 67 (7) C-144 (1984)

64. Y. Tree, A. Venkateswaran, D. P. H. Hasselman, "Observations on the Fracture and Deformation Behavior During Annealing of Residually Stressed Polycrystalline Aluminum Oxides", J. Mat. Sci. 18, 2135-48 (1983)

65. T. J. Chuang, "Estimation of Power-Law Creep Parameters from Bend Test Data", J. Mat. Sci. 21, 165-75 (1986)

66. S. I. Warshaw and F. H. Norton, "Deformation Behavior of Polycrystalline Aluminum Oxide", J. Amer. Ceram. Soc. 45, 479-86 (1962)

67. R. L. Coble and Y. H. Guerard, "Creep of Polycrystalline Aluminum Oxide", J. Amer. Ceram. Soc. 46, 353-54 (1963)

68. A. Crosby and P. E. Evans, "Creep in Pure and Two-Phase Nickel-Doped Alumina", J. Mat. Sci. 8, 1573-78 (1973)

69. R. M. Arons, J. K. Tien, "Creep and Strain Recovery in Hot-Pressed Silicon Nitride", J. Mat. Sci. 15, 2046-58 (1980)

70. T. Fett and D. Munz, "Determination of Transient Creep Parameters of HPSN by Dynamic Bending Tests", J. Mat. Sc. 19, 1791-98 (1984)

71. T. Fett and D. Munz, "Determination of Crack Growth Parameter N in Ceramics Under Creep Conditions", J. Test. and Eval. 3, 143-51 (1985)

72. S. M. Wiederhorn, "Subcritical Crack Growth in Ceramics", pp. 613-46 in Fracture Mechanics of Ceramics, Vol. 2, ed. by R. C. Bradt, D. P. H. Hasselman and F. F. Lange, Plenum Press, New York, N. Y. (1974)

73. D. P. H. Hasselman, A. Venkateswaran, "Effect of Cracks on Mechanisms and Kinetics of Creep Deformation of Brittle Materials", pp. 525-45 in Deformation of Ceramic Materials II, ed. by R. E. Tressler and R. C. Bradt, Plenum Press (1984)

74. R. F. Canon, J. T. A. Roberts and R. J. Beals, "Deformation of UO_2 at High Temperatures", J. Amer. Ceram. Soc. 54 (2) 105-112 (1971)

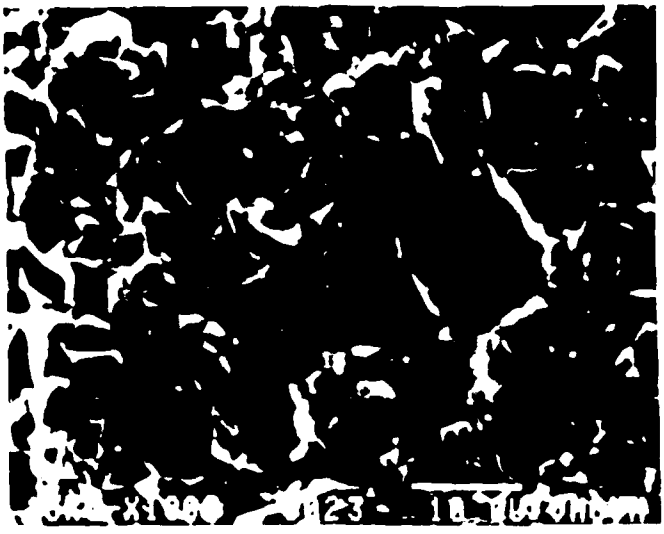

Fig. 1. SEM-fractograph of AlSiMag 838 alumina fractured at room temperature.

Fig. 2. Scanning-electron-micrograph of polished section of undeformed 838 alumina.

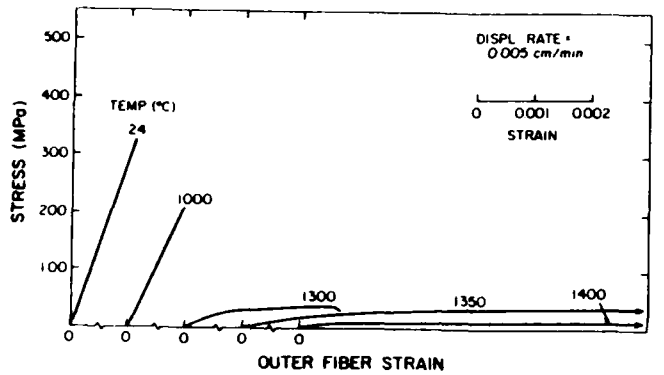

a.

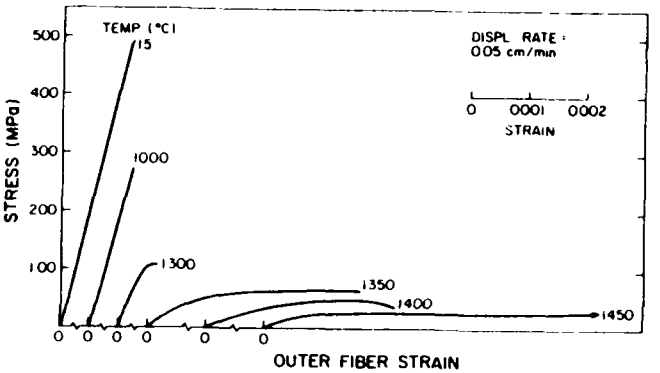

b.

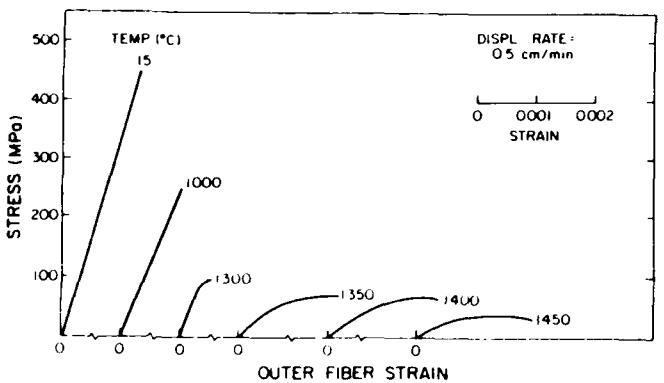

c.

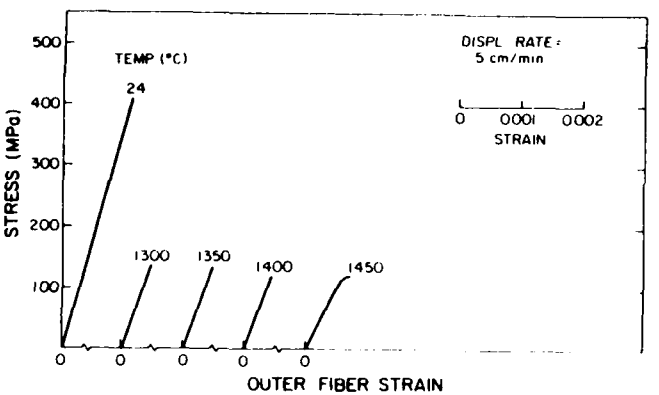

d.

Fig. 3. Stress-strain behavior of 838 polycrystalline alumina over range of temperature at displacement rates: a, 0.005 cm/min; b, 0.05 cm/min; c, 0.5 cm/min and d, 5 cm/min.

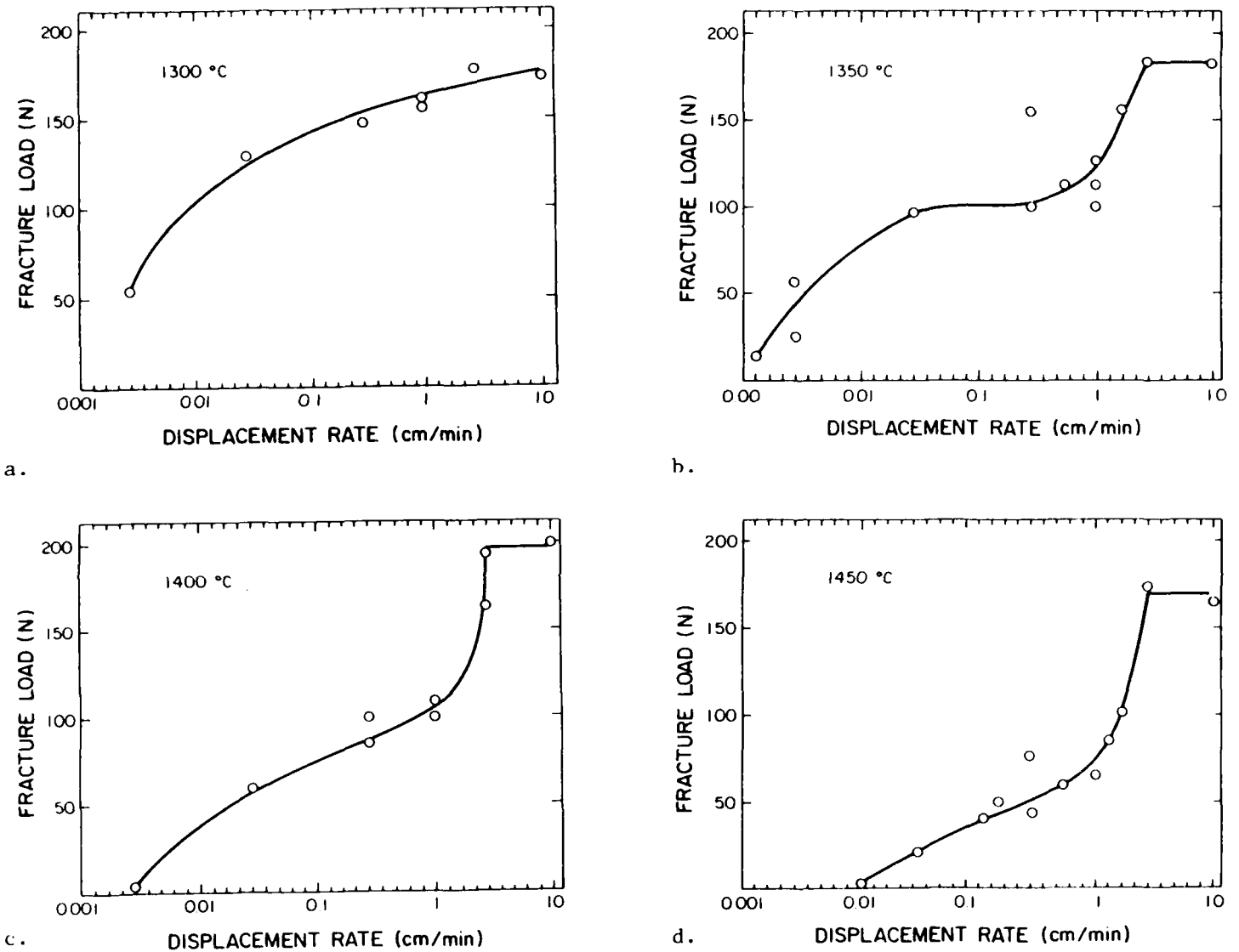

Fig. 4. Dependence of maximum creep or fracture load on displacement rate for 838 alumina deformed at: a, 1300°C; b, 1350°C; c, 1400°C and d, 1450°C.

a.

b.

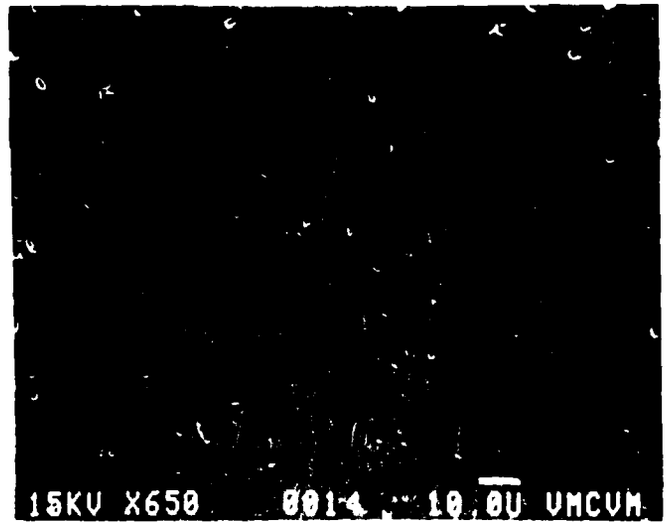

Fig. 5. Scanning [illegible] polished sections of 838 alumina [illegible] ement rates: a, 0.005 [illegible].

a.

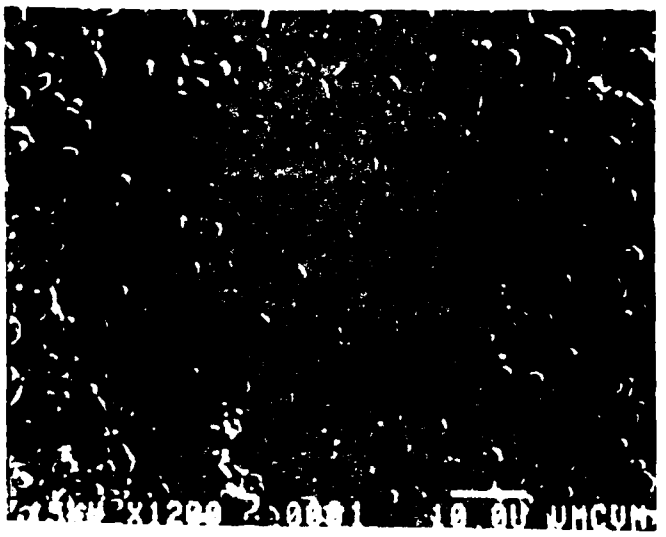

b.

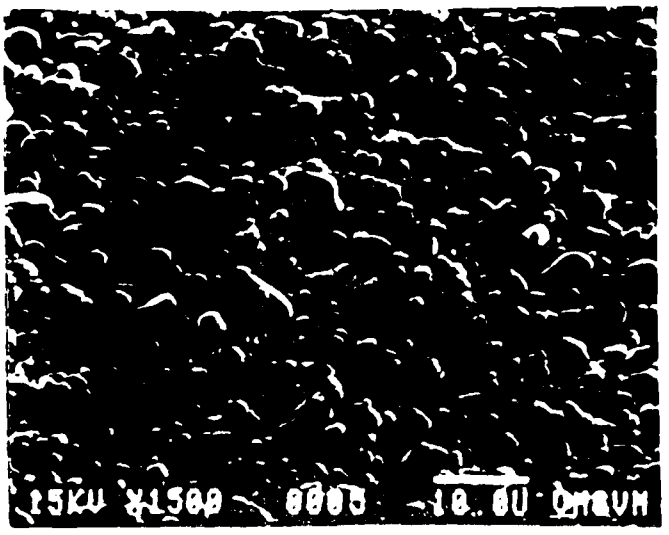

Fig. 6. Scanning [illegible] tensile surfaces of 838 alumi[illegible] at displacement rates: a, 0.005 [illegible].

Fig. 7. Scanning electron fractograph of 838 alumina broken at 1300°C at displacement rate of 0.05 cm/min

a.

b.

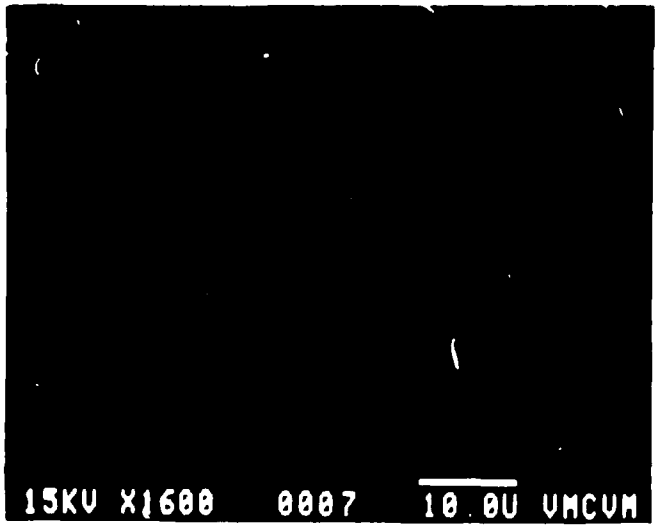

c.

Fig. 8. Scanning electron micrographs of polished sections of 838 alumina deformed at 1350°C at displacement rates: a, 0.005 cm/min; b, 0.5 cm/min and c, 5 cm/min. (Tensile edge at right of figure).

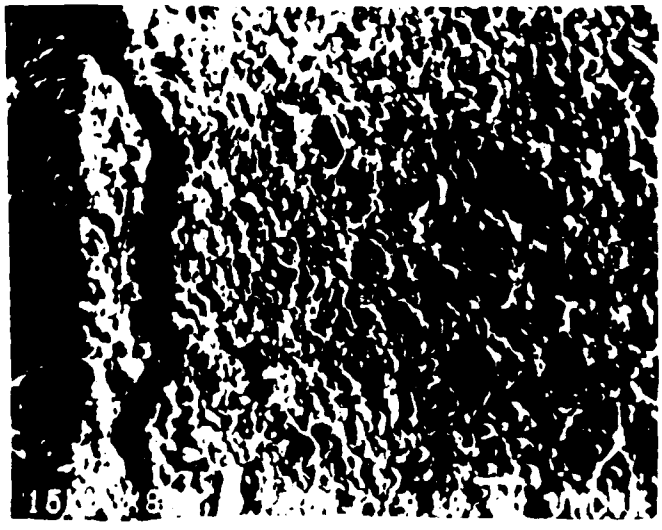

Fig. 9. Scanning electron micrograph of tensile surface of 838 alumina deformed at 1350°C at displacement rate of 0.5 cm/min.

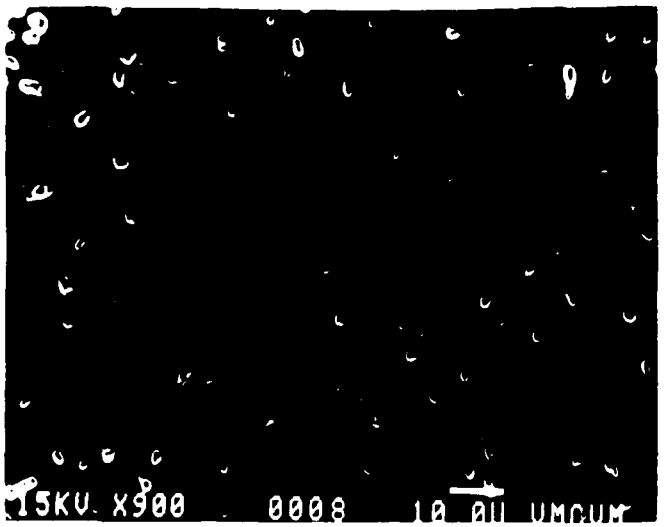

a.

b.

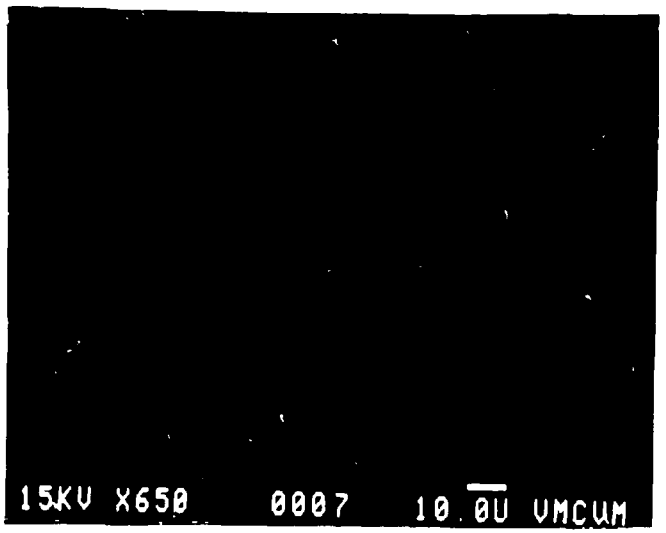

c.

Fig. 10. Scanning electron micrographs of polished sections of 838 alumina deformed at 1400°C at displacement rates: a, 0.005 cm/min.; b, 0.5 cm/min. and c, 5 cm/min. (Tensile edge at right-hand side of figure).

Figure 11. Scanning electron micrograph of tensile surface of 838 alumina deformed at 1400°C at displacement rate of 0.5 cm/min.

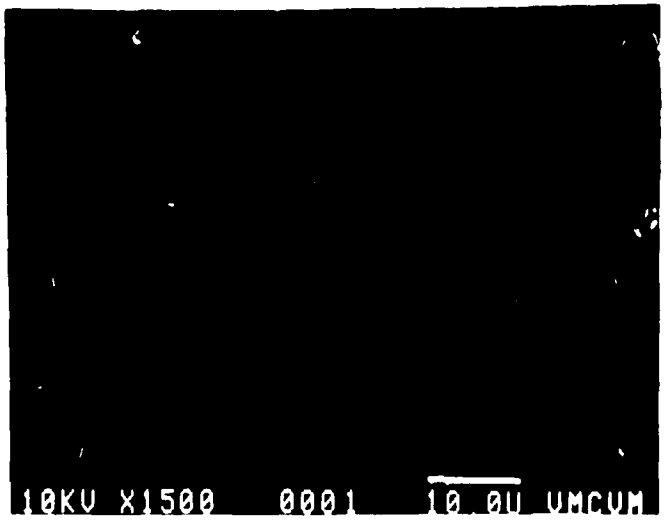

a.

b.

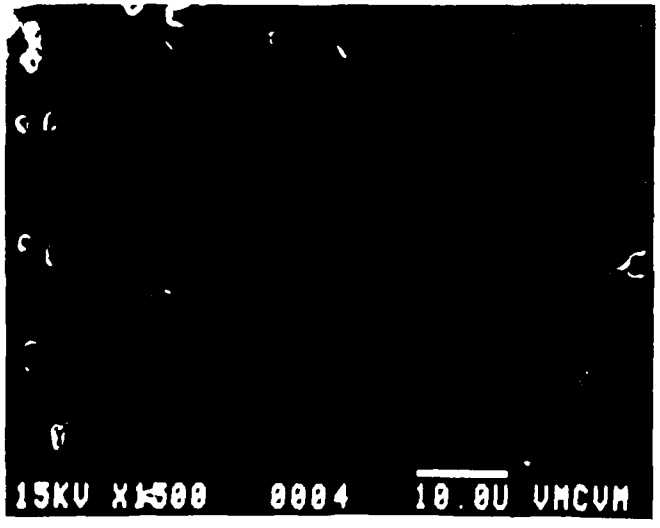

c.

Fig. 12. Scanning electron micrographs of polished sections of 838 alumina deformed at 1450°C at deformation rates: a, 0.01 cm/min.; b, 0.5 cm/min. and c, 10 cm/min. Tensile edge at right hand side of figures.

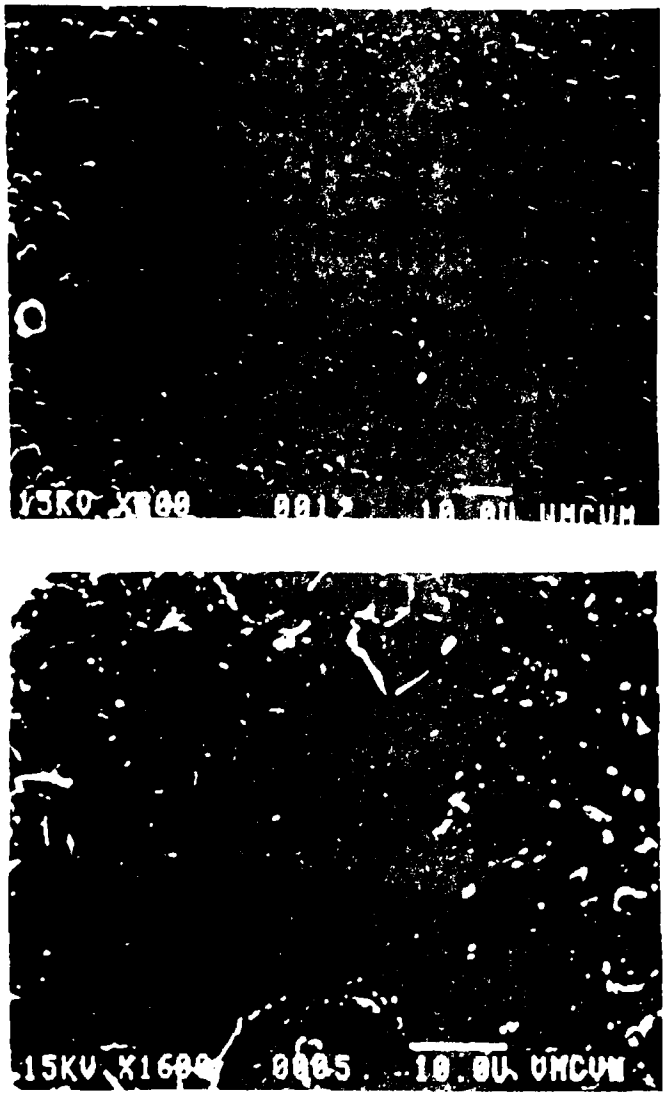

Fig. 13. Scanning electron [illegible] tensile surface of 838 alumina [illegible] at displacement rates: a, [illegible]; [illegible].

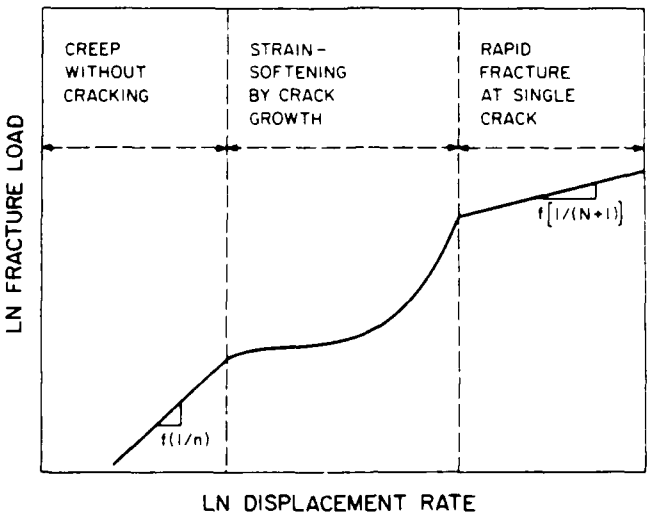

Fig. 14. Schematic representation of three regimes for dependence of failure load on displacement rate.

Contribution of damage by multiple crack growth to the strain-rate sensitivity of a polycrystalline alumina at elevated temperatures

D. P. H. HASSELMAN, A. VENKATESWARAN, K. Y. DONALDSON
Department of Materials Engineering, Virginia Polytechnic Institute and State University, Blacksburg, Va. 24061, USA

ABSTRACT

The strength of a polycrystalline aluminum oxide measured in 4-point bending at elevated temperatures over a range of displacement-controlled loading rates was observed to exhibit an unusually high strain-rate dependence. Scanning electron microscopy revealed that at the lower values of strain rate failure was accompanied by the formation of a number of additional macrocracks adjacent to the plane of fracture. Separate measurements of specimens deformed to approximately 75% of the fracture strain indicated that, at these lower values of strain rate, the effective Young's modulus was decreased by as much as a factor of two. It is suggested that the high strain-rate sensitivity was the direct result of a strain-rate dependent decrease in Young's modulus and associated effect of "strain-softening" for conditions of displacement-rate controlled mechanical loading. The validity of this hypothesis was verified by a fracture-mechanics analysis of a mechanical model subjected to displacement-controlled tensile loading, with elastic behavior expressed in terms of the effect of cracks on continuum elastic properties.

1. Introduction

Brittle materials at stress levels below the instantaneous fracture stress exhibit slow crack extension, referred to as "sub-critical crack growth", with a rate strongly dependent on environmental conditions such as humidity and temperature [1]. Under conditions of dynamic loading, such as constant stress or strain-rate testing, sub-critical crack growth leads to a loading-rate dependence of the failure stress, generally referred to as "strain-rate sensitivity" [2-5].

In principle, the "strain-rate sensitivity" of a given material can be derived on the basis of well-known principles of fracture mechanics, provided that information exists on the crack growth behavior, the critical stress intensity factor and the crack-size geometry and/or instantaneous fracture stress [6, 7]. In doing so, however, a careful distinction must be made between loading conditions of constant stress rate and constant strain rate. The presence of a crack, depending on its size relative to the specimen size, can have a significant effect on the compliance of the specimen. For constant stress rate loading conditions, any change in specimen compliance due to crack growth is corrected for automatically by the appropriate instrumentation, such as that found in servo-electric-hydraulic mechanical testers, so that the sample loading rate is not affected by a change in specimen compliance. However, under conditions of constant strain rate, usually achieved with the aid of displacement-controlled mechanical testers, at any given value of displacement an increase in specimen compliance will cause a corresponding decrease in the applied load and loading rate.

The role of specimen compliance in crack propagation behavior is well recognized in the general field of fracture mechanics and in evaluation of crack propagation behavior and fracture toughness [8,9,10]. Furthermore, Evans [7] analyzed the effect the increase in specimen compliance due to the sub-critical growth of a single failure-initiating flaw has on strain-rate sensitivity. The results of this analysis showed that for crack sizes at failure, l_f, less than 10 % of the specimen thickness, W, the increase in specimen compliance is sufficiently small that the stress-rate and strain-rate are simply related by Young's modulus of the material of the test specimen such that the stress-rate sensitivity of the failure stress can be obtained with the use of displacement (strain)-controlled mechanical testers and vice-versa. For $l_f > .1$ W, however, the stress rate and strain rate can no longer be related simply by Young's modulus and the effect of increased compliance must be taken into account when using constant displacement rate tests to obtain strain-rate sensitivity data.

Rather than failing from the formation and growth of a single crack, many brittle materials can undergo simultaneous growth of a number of cracks. Such multiple cracks can arise from a number of sources, such as surface damage [11] or processing flaws [12]. High densities of microcracks can form, either spontaneously or under the influence of an applied stress, as the result of internal stresses due to a spatially non-uniform thermal expansion in polycrystalline single-phase materials [13] or brittle matrix composites [14]. Cracks can also be initiated at stress concentrations in heterogeneous materials such as concrete [15] and rock [16]. At elevated temperatures microcrack formation can result from grain boundary sliding [17], stress-induced growth of residual pores or by

cavitation [18]. Coalescence of such microcracks can result in the formation of macrocracks.

The presence of cracks, as demonstrated analytically and experimentally, can cause a significant lowering of the effective elastic moduli of materials [19-23]. For this reason, multiple crack formation and/or growth should lead to an increase in the compliance of the mechanical test specimens of brittle materials. This effect, in brittle materials which do not deform plastically, such as concrete and rock, when subjected to mechanical loading at a constant displacement rate, leads to a type of non-linear stress-strain behavior referred to as "strain-softening", i. e., a decrease in the value of the load at any given value of displacement compared to the value expected from Young's modulus of the untested crack-free materials [15, 16, 24, 25].

In a recent study by the present writers [26], which focussed on the fractography of the role of cracks in the non-linear deformation of polycrystalline ceramics, it was found that the fracture stress exhibited what appeared to be a rather high strain-rate sensitivity. Furthermore, it was noted that deformation was accompanied also by a strain-rate dependent formation of multiple macrocracks along the lengh of the specimen, in addition to the formation of the failure-causing crack. It was speculated that the formation of these macrocracks and associated increase in specimen compliance could explain, at least in part, the observed high strain-rate sensitivity.

The purpose of this investigation was to conduct an experimental study of this effect and to present an analysis for conditions of uniaxial tensile loading.

2. Experimental

2.1. Material

The test material chosen for this study consisted of a substrate-quality, relatively fine-grained polycrystalline aluminum oxide known as AlSiMag 838*. The scanning electron micrograph of a room temperature fracture surface shown in fig. 1 indicates that this material is nearly fully dense with an average grain size of ~5 μm and an occasional grain as large as 20μm. For purposes of future comparison, fig. 2 shows a scanning electron micrograph of a polished section through an annealed undeformed specimen, which indicates the presence of an occasional pore without any preferred pore orientation.

The test samples were circular rods with a length of ~50 mm and a diameter of ~4.8 mm. Prior to testing all samples were annealed at about 1000 ^{o}C for 6-7 hr to minimize the effect of residual stresses, if any.

2.2. Test procedures

The specimens were tested in 4-point bending with inner and outer spans of 10 and 40 mm, resp. The specimen holder consisted of graphite, the load to the specimens being transferred by graphite pins which were permitted to rotate freely in order to keep extraneous stresses to a minimum. Testing was done in an argon atmosphere within an environmental chamber resistively heated with tungsten mesh heating elements. The environmental chamber was contained within the load-frame of an electro-hydraulic closed-loop mechanical tester made by the MTS Corporation. The displacement of the actuator and the resulting load were transferred via

---

* General Electric Corp., Chattanooga, Tennessee, USA

graphite push-rods and water-cooled bellows to the specimen and load cell, resp. The displacement of the actuator was measured using a displacement gauge, held against the actuator outside the environmental chamber. This gauge, with a range of ~4 mm, permitted measurement of the displacement to within a few μm. By making a separate measurement of the elastic displacement of the total load train without the specimen, the displacement of the loading points of the specimens could be obtained by the appropriate subtraction. For the test material and specimen size of this study, the elastic displacement of the specimen and load train were approximately equal in value. The load as a function of displacement was recorded with an x-y recorder for most values of displacement rate and with an oscilloscope at the highest values of displacement rate. For purposes of measuring the strain-rate sensitivity, the specimens were loaded over a range of values of constant displacement rates at temperatures of 1350, 1400 and 1450 ^{o}C. The displacement-load data were converted to strain and stress using the theory for pure bending of homogeneous beams.

In order to determine possible changes in the effective Young's modulus during deformation, specimens were deformed at 25, 1400 and 1450^{o}C over the lower range of strain rates (0.0016 to 0.08 min^{-1}) to approximately 75 to 85% of the failure strain observed in the fracture studies. The effective Young's modulus at room temperature of these deformed samples was then obtained from load-displacement data obtained from four-point bending tests identical to the deformation at high temperature. Changes in Young's modulus for strain rates in excess of 0.08 min^{-1}, could not be obtained due to experimental difficulties encountered in deforming the specimens to prescribed small values of displacement. Possibly because of scattering at

the cracks which formed during high temperature deformation, Young's modulus could not be measured by acoustic techniques.

Following testing, the specimen external and fracture surfaces (if broken) were examined by scanning electron microscopy. The specimens were also sectioned by a slow-speed diamond saw and then diamond-polished to provide a crossection of the specimen interior ranging from the line of maximum tensile stress to the line of maximum compressive stress.

3. Results and discussion.

3.1. Deformation, fracture stress and fractography

Figs. 3a, b and c show typical stress-strain behavior for a range of values of strain rate at 1350, 1400 and 1450 ^{o}C, resp. Considerable non-linearity can be noted. Fracture resulted for all but the lowest values of strain rate, at which the stress developed did not exceed the failure stress over the duration of the experiment. It should also be noted that a number of stress-strain curves just prior to fracture showed a decrease in stress with increasing strain. This latter effect is not expected for generally accepted mechanisms of creep, but in the absence of major changes in specimen geometry, as is the case in this study, can result only from an increase in specimen compliance, due to be discussed subsequently.

Figs. 4a, b and c show the magnitude of the failure stress for the specimens which exhibited fracture as a function of strain rate, calculated from the displacement rate, and plotted on a log-log basis for 1350, 1400 and 1450 ^{o}C, resp.

Experimental data for the failure stress as a function of loading rate can be used to evaluate the magnitude of the stress intensity exponent, N,

in the dependence of the rate of sub-critical crack growth, V, on the stress-intensity factor, K_I [6]. Initially the assumption will be made that the cracks do not significantly affect the specimen compliance, such that the strain rate, $\dot{\varepsilon}$, is given by:

$$\dot{\varepsilon} = \dot{\sigma}/E_o \tag{1}$$

The relationship of sub-critical crack velocity, V, and mode I stress-intensity factor, K_I, was assumed to be:

$$dl/dt = AK_I^N \tag{2}$$

where N is the stress-intensity factor exponent.

The dependence of the fracture stress, σ_f, on strain rate (for certain simplifying assumptions discussed in the original studies [6]) can be derived to be:

$$\sigma_f^{N+1} = CE_o\dot{\varepsilon} \tag{3}$$

where C is a constant for a given material and environment.

Eq. 3 indicates that the slope of the plot of log (σ_f) vs. log ($\dot{\varepsilon}$) equals 1/(N + 1). This relationship, for the slopes of the data in figs. 4a, b and c, yields values of N equal to 5, 2.7 and 2.3 for 1350, 1400 and 1450 ^{o}C, resp. These values generally are far lower than those obtained for alumina and other brittle materials at ambient or elevated temperatures [4, 7, 27-31].

Scanning electron microscopy of the surfaces of the fractured specimens revealed that deformation was accompanied by a strain-rate dependent formation of cracks adjacent to the plane of fracture.

Figs. 5a and b show polished sections of specimens deformed at 1350 ^{o}C at strain rates of 0.08 and 0.8 min^{-1}, resp., with the right-hand side of the figure at or near the line of maximum tensile stress. The specimen deformed at the lower value of strain rate shows some evidence for

intergranular cracking perpendicular to the tensile stress, whereas such crack formation is absent in the specimens deformed at 0.8 min^{-1}.

Fig. 6 shows a scanning electron-micrograph of the tensile specimen surface adjacent to the plane of fracture of the same specimen shown in fig. 5a. The specimen surface gives evidence for development of at least two additional cracks in addition to the plane of fracture. One such crack appears to have been nucleated at a large grain.

As indicated by their dimensions relative to the scale of the microstructure as well as their preferred path of propagation, crack formation in the alumina tested under the conditions of this study appears to occur by the growth of macrocracks along the grain boundaries rather than by the formation of isolated intergranular cracks of the order of the grain size, such as those observed by Folweiler and others [31, 32]. No crack formation could be detected in the regions of the specimen of fig. 5a and 6 subjected to compressive loading.

Figs. 7a and b show polished sections of specimens deformed at ~1400°C at strain rates of 0.08 and 0.8 min^{-1}, resp. Again, crack formation was found only at the lower strain rate, and was absent at the higher value. A surface crack in the specimen deformed at 0.08 min^{-1} is shown in fig. 8.

At 1450 °C crack formation was extensive, as indicated by SEM-micrographs of sections of the specimen interiors and surfaces shown in figs. 9 and 10, resp. Crack formation occurred at strain rates of 0.08, 0.16 and 0.32 min^{-1}, but was absent at 1.6 min^{-1}. For all three temperatures the number of cracks which formed along the central portion of the bend-specimen ranged from two to four.

In general, the microstructural evidence suggests that multiple crack formation in those specimens which exhibited fracture occurred at the lower

values of strain rate, but was absent (or could not be detected) at the higher values of strain rate. Furthermore, crack formation appeared to be more pronounced at 1400 and 1450 ^{o}C than at 1350 ^{o}C. In terms of a possible interpretation of these results, it should be noted that no crack formation could be detected in those specimens deformed at the lowest strain rates, which did not exhibit fracture over the time period of the deformation and for which no strength data could be obtained. It is postulated that for these specimens, the strain rate was sufficiently low that deformation could occur by diffusional creep at stress levels below those required for crack nucleation. It appears, then, that crack formation occurred only over the intermediate values of strain rate of this study, at which the stress exceeded the minimum value required for multiple crack nucleation and for which the time to failure was sufficiently long for significant crack propagation to occur.

Fig. 11 shows the data for the effective Young's modulus of specimens deformed at 25, 1400 and 1450^{o}C, over a range of strain rates up to 0.08 min^{-1}, to approximately 75 and 85% of the fracture strain established during the measurements of the strain-rate sensitivity. The data obtained at 25^{o}C shows an average value, independent of strain rate, of ~400 GPa which compares very favorably with general literature values for Young's modulus of fully dense polycrystalline aluminum oxide. The absence of an effect of strain rate on Young's modulus is reflective of the absence of any microstructural changes during deformation at 25^{o}C.

At 1400 and 1450^{o}C, however, a pronounced loading rate effect is present. This is especially so for the data at 1450^{o}C where Young's modulus is decreased from the value for the crack-free material by as much as a factor of two at the lowest value of strain rate. This must have a

significant effect on the magnitude of stress reached under the conditions of displacement controlled loading of this study. For 1400°C, Young's modulus of the specimens deformed to ~85% of the failure strain is some 10% below the value for the specimens deformed to ~75% of the failure strain. This effect does not appear to be present for the data of the specimens deformed at 1450°C.

Extrapolation of the data for Young's modulus following deformation at 1400 and 1450°C to higher values of strain rate suggests that a strain rate of ~0.2 min^{-1} would result in a value of Young's modulus ~400 GPa, as found for the crack-free material. This implies that no significant multiple crack formation would occur at strain rates > 0.2 min^{-1}, which confirms the fractographic evidence presented earlier that no crack formation occurred at the higher values of strain rate of this study.

It should be pointed out that the data shown in fig. 11 represent the effective Young's modulus at strains of ~75 and ~85% of the fracture strain. It is speculated that if data could have been obtained for specimens deformed to within a few percent of the failure strain, they may well have been significantly lower.

In view of the above observations, at least two explanations can be given for the high strain-rate sensitivity, i.e., low values of N for the failure stress as observed in this study. Firstly, prior to fracture, the specimen can deform by creep. Under conditions of loading by a constant strain rate, if the fracture and creep processes are independent, creep deformation will result in a lower stress value than would have been obtained in the absence of creep. Because the total amount of creep deformation at any given temperature prior to fracture will decrease with increasing displacement rate, an enhancement of the dependence of fracture

stress on strain rate is expected, thereby resulting in a decrease in the apparent value of N.

The second explanation for low values of N is based on the effect sub-critical growth of multiple cracks has on the compliance of the specimen prior to fracture. Here, as for creep deformation, the relative amount of the sub-critical growth of multiple cracks and resulting increase in specimen compliance as manifested by the decrease in effective Young's modulus and associated decrease in stress will increase with decreasing strain rate. In turn, this will decrease the apparent value of the stress intensity exponent N obtained from the experimental data for the strain rate sensitivity. The results for the fractography and the observed strain-rate dependent decrease in Young's modulus provide supporting evidence for the latter hypothesis.

Consequently, the observed strain-rate sensitivity is expected to be governed by the combined effects of diffusional creep and strain-rate dependent "strain-softening". An estimate of the relative contribution of both these effects may be difficult to evaluate. Nevertheless, an estimate can be obtained of the stress-strain response in the absence of crack formation assuming deformation occurs by the dominant mechanism of diffusional creep, which for the mean grain size and temperature of the alumina of this study occurs by Coble creep controlled by diffusion of the Al^{3+} ion [34]. The creep rate ($\dot{\varepsilon}_c$) at any given value of stress (σ) is expressed by:

$$\dot{\varepsilon}_c = 24 \sigma \Omega D_{gb} / d^3 kT \qquad (4)$$

where the symbols and numerical values taken from the study of Langdon and Mohamed [34] are: σ is the applied stress, Ω is the molecular volume = $4.2 \times 10^{-29} m^3$, d is the grain size = 5 μm, k = Boltzmann constant = 1.38 x

10^{-23} J/atom ^{o}K, T = absolute temperature (1673 ^{o}K used for calculations), D_{gb} is the grain boundary diffusivity for the Al^{3+} ion = $8.6 \times 10^{-10} \exp(-419{,}000/8.314\ T)$.

For constant strain rate $\dot{\varepsilon}$, the dependence of stress on time, t, can be derived to be

$$\sigma(t) = \eta\dot{\varepsilon}_c[1 - \exp(-E_o t/\eta)] \qquad (5)$$

where η is the effective viscosity with $\eta = \sigma/\dot{\varepsilon}$.

The stress response for a material subjected to a constant strain rate and associated creep response given by eq. 4 was calculated for the range of strain rates and specimen configuration of this study.

Fig. 12 shows the results obtained. Comparison with the stress-strain results presented in fig. 3 shows that in the absence of cracks the stress reached far exceeds the values observed in this study. Even if eq. 4 were in error by as much as an order of magnitude, it can be concluded that diffusional creep made only a minor contribution to the stress-strain behavior at the intermediate values of strain rate, leaving the effect of strain-softening due to crack formation as the primary mechanism.

3.2. Analysis

The mechanical model selected for this analysis consisted of a linearly elastic solid containing non-interacting penny-shaped cracks of equal size, oriented perpendicularly to a uniaxially applied tensile stress. In analogy to earlier studies of the effect of cracks on continuum elastic properties, Young's modulus (E) of the cracked solid was assumed to be described by:

$$E = E_o\ (1 + \ )^{-1} \qquad (6)$$

where E_o is Young's modulus of the crack-free material. For parallel

penny-shaped cracks oriented perpendicularly to the applied stress, the quantity, α [22] is given by:

$$\alpha = 16\ (1-\nu_o^2)\ N_c l^3/3 \tag{7}$$

where ν_o is Poisson's ratio of the crack-free material, N_c is the number of cracks per unit volume and l is the radius of the cracks, where $l = l(t)$ and t is the time. At $t = 0$, the initial value for α is taken as α_o.

The model was assumed to be initially stress-free and subjected to deformation under a constant strain rate, $\dot{\varepsilon}$, at $t = 0$.

The stress, $\sigma(t)$, becomes:

$$\sigma(t) = \dot{\varepsilon} t E_o\ (1+\alpha)^{-1} \tag{8}$$

The stress intensity factor, K_I, stress, $\sigma(t)$, and crack size, l, are related by:

$$K_I = Y\sigma l^{1/2} \tag{9}$$

where Y is a geometric constant, which from the solution of Sack for a penny-shaped crack [35] can be derived to be equal to $2(1-\nu_o^2)^{1/2} / \pi^{1/2}$.

Substitution of eqs. 8 and 9 into eq. 2 yields:

$$\int_{l_c}^{l} dl/dt = AY^N \dot{\varepsilon}^N t^N E_o^N l^{N/2}\ (1+\alpha)^{-N} \tag{10}$$

which reduces to:

$$(1+\alpha)^{N-N/2} dl = AY^N \dot{\varepsilon}^N E_o^N t^{N+1}/(N+1) \tag{11}$$

A solution for the integral in eq. 11 can be obtained from the tables compiled by Groebner and Hofreiter [36]. This solution, too complex for reproduction here, was programmed for computer evaluation to yield the crack size, l, σ and E, as a function of the time of loading. The value of stress, $\sigma(t)$, was calculated with the aid of eq. 8.

Failure was predicted on the basis of the criterion:

$$K_I = K_{IC} \tag{12}$$

where K_{IC} is the critical stress intensity factor, with the fracture

stress, σ_f, defined as:

$$\sigma_f = K_{IC} Y^{-1} l_f^{-1/2} \tag{13}$$

where l_f refers to the crack size at fracture.

The analytical results presented above are illustrated by means of a numerical example for a polycrystalline aluminum oxide at 1400 °C with property data and other parameter values as listed in Table 1, obtained from various literature sources [27, 37, 38]. The values of K_{IC} and N at 1400 °C were obtained by a linear extrapolation of literature data. Because the SEM-micrographs show the cracks to be much larger than the grain size, the value of the initial crack radius was arbitrarily chosen as equal to 50 μm.

Figs. 13a, b, c and d, for the arbitrarily selected initial value of α_o = 0.05, show the stress-strain curves for values of the strain-rate equal to 3, 3 x 10^{-2}, 9 x 10^{-3} and 3 x 10^{-3} min^{-1}, resp,calculated with the aid of eqs. 8 and 11. Included in the figures is the decrease in fracture stress with increasing strain, resulting from the amount of crack growth calculated from eq. 13. Fracture at $K_I = K_{IC}$ occurs at the value of strain which corresponds to the intersection of the two curves. At the highest value of strain rate the time to failure is sufficiently short so that no significant crack growth has occurred. As a result, the stress-strain curve in fig. 13a is linear and the fracture stress is invariant with increasing strain. At the somewhat lower strain-rate of 3 x 10^{-2}, the stress-strain curve exhibits a slight degree of non-linearity, accompanied by a small decrease in fracture stress with increasing strain. At the even lower strain rate of 9 x 10^{-3} min^{-1}, as shown in fig. 13c, just prior to failure the stress exhibits a decrease with increasing strain. At the lowest value of strain rate, this decrease in stress with increasing strain

is such that the stress-strain curve never intersects the curve for the strain dependence of the fracture stress. Therefore for this value of strain rate the condition of failure at $K_I = K_{IC}$ is never reached. The cracks will propagate sub-critically only, with specimen separation occurring when the cracks have traversed a distance equal to the dimension of the specimen.

Fig. 14 is a log-log plot of the fracture stress as a function of strain rate, for values of α_o ranging from 0 to 0.1. At the highest values of strain-rate of > 0.3 min^{-1}, the fracture stress is almost independent of the strain rate and the value of α_o, because the time-to-failure is too short to permit significant crack growth. Over the range of lower values of strain rate, the fracture stress is reduced significantly, the relative decrease increasing with increasing value of α_o. Also indicated in fig. 14 is the minimum value of strain rate at which failure still occurs at $K_I = K_{IC}$. Below this value of strain rate the cracks will propagate sub-critically only, as discussed earlier in the context of the stress-strain and fracture stress-strain curves shown in fig. 13d.

As discussed earlier, the slope of the log fracture stress-log strain rate curve yields the value for the critical stress intensity factor exponent, N. However, the curves in fig. 14 indicate that at any given value of strain rate the value of the slope depends strongly on the value of α_o. The magnitude of the slope increases strongly with increasing value of α_o, i. e., with the degree to which the magnitude of the failure stress is affected by multiple crack growth.

Using eq. 3, an equation that ignores the effect of multiple crack growth, to calculate N for $\alpha_o = 0$ and the strain-rates given in fig. 14, a value of N = 10 (the value used to generate the curves) is calculated only

for the lowest value of strain rate. However, at the lowest values of strain rate for which failure still occurs at $K_I = K_{IC}$ and higher values of α_o, i. e., α_o = .02, .05 and 0.1, eq. 3 predicts N values of 6.1, 2.7 and 1.5, resp., all far less than the actual value of N = 10. These results indicate that the value of N can be grossly underestimated if the effect of crack formation is ignored when calculating N.

Although direct quantitative comparisons between the experimental data and the analytical model should be approached with caution, both indicate that multiple crack formation and associated strain-softening can contribute significantly to the strain-rate sensitivity of the failure stress.

In general, it is expected that the relative contributions of creep and crack growth will vary from material to material. For purposes of a quantitative comparison between experimental and calculated values of N an analysis for deformation in bending is required, which requires detailed information on the spatial variation of Young's modulus and the shift in position in the neutral axis as crack growth proceeds. Also, due to the usual assumption that plane sections remain plane, the deformation by creep and crack formation in the cracked tensile zone is expected to be coupled with the diffusional creep within the regions of the specimen subjected to compressive stress. Such an analysis is outside the scope of the present investigation.

The results of this study suggest that in studies of the deformation and fracture of polycrystalline structural ceramics at elevated temperatures, it is essential that the extent of multiple crack formation be established for proper quantitative interpretation of the experimental data. Such crack formation not only is expected to affect the strain-rate

sensitivity, as suggested by the results of this study, but also the creep characteristics under constant load [39-41].

Acknowledgment.

This study was supported by the Army Research Office under Contr.: DAAG 29-85-K-0106.

References.

1. Fracture Mechanics of Ceramics, Vols. 1-8, ed. by R. C. Bradt, A. G. Evans, D. P. H. Hasselman, F. F. Lange. Plenum Press, New York, N. Y. (1974, 1978, 1983, 1986)
2. J. E. Ritter, Jr., M. S. Cavanaugh, J. Amer. Ceram. Soc. 59 (1976) 57
3. J. T. A. Pollock, G. F. Hurley, J. Mat. Sci. 8 (1973) 1595
4. J. E. Ritter, Jr., J. N. Humenik, J. Mat. Sci. 14 (1979) 626
5. J. E. Ritter, Jr., G. S. Glaesemann, K. Jakus, P. Rampone, Physics and Chemistry of Glasses 27 (1986) 65
6. J. E. Ritter, Jr., pp. 667-86 in Fracture Mechanics of Ceramics, Vol. 4, ed. by R. C. Bradt, D. P. H. Hasselman, F. F. Lange, Plenum Press, N. Y. (1978)
7. A. G. Evans, Int. J. of Fracture 10 (1974) 251
8. G. Sih, Methods of Analysis and Solutions for Crack Problems, Mechanics of Fracture, I, Noordhoff, Leiden (1973)
9. H. L. Ewalds, R. J. H. Wanhill, Fracture Mechanics, Edward Arnold Publishers, London, Baltimore (1983)
10. K. Hellan, Introduction to Fracture Mechanics, McGraw-Hill (1984)
11. A. G. Evans, pp. 303-31 in Fracture Mechanics of Ceramics, Vol. 3, ed. by R. C. Bradt, D. P. H. Hasselman, F. F. Lange, Plenum Press, New

York, N. Y. (1978)

12. A. G. Evans, pp. 475-502 in Proc. of the Sixth Army Materials Technology Conference; Ceramics for High-Performance Applications III: Reliability, ed. by E. M. Lenoe, R. N. Katz and J. J. Burke, Plenum Press, New York, N. Y. (1983)
13. A. G. Evans, Acta Metall. 26 (1978) 1845
14. F. F. Lange, pp. 599-612 in Fracture Mechanics of Ceramics, Vol. 2, ed. by R. C. Bradt, D. P. H. Hasselman and F. F. Lange, Plenum Press, New York, N. Y. (1974)
15. Z. P. Bazant, J. Eng. Mech. Div., ASCE 102 (1976) 331
16. Z. P. Bazant, B. H. Oh, J. Eng. Mech. Div., ASCE 110 (1984) 1015
17. A. G. Evans, Acta Metall. 28 (1980) 1155
18. T. J. Chuang, K. I. Kagawa, J. R. Rice and L. B. Sills, Acta Metall. 27 (1979) 265
19. J. B. Walsh, J. Geophys. Res. 70 (1965) 381
20. R. L. Salganik, Izv. Akad. Nauk. SSR, Mekh. Tverd, Tela. 8 (1973) 149
21. B. Budiansky, R. J. O'Connell, Int. J. Solid Struct. 12 (1976) 81
22. D. P. H. Hasselman and J. P. Singh, Amer. Ceram. Soc. Bull. 58 (1979) 856
23. J. A. Kuszyk and R. C. Bradt, J. Amer. Ceram. Soc. 56 (1973) 420
24. E. P. Chen, L. M. Taylor, pp. 175-86 in Fracture Mechanics of Ceramics, Vol. 7, ed. by R. C. Bradt, A. G. Evans, D. P. H. Hasselman, F. F. Lange, Plenum Press, New York, N. Y. (1986)
25. R. M. L. Foote, Y.-W. Mai, B. Cotterell, J. Mech. Phys. Solids 34 (1986) 593
26. K. Y. Donaldson, A. Venkateswaran, D. P. H. Hasselman, Proc. Conference on Fractography of Glasses and Ceramics. American Ceramic Society (in

press)

27. K. Jakus, T. Service and J. E. Ritter, Jr., J. Amer. Ceram. Soc. 63 (1980) 4

28. R. F. Pabst, G. Popp, pp. 305-15 in Fracture Mechanics of Ceramics, Vol. 5, ed. by R. C. Bradt, A. G. Evans, D. P. H. Hasselman and F. F. Lange. Plenum Press, New York, N. Y. (1983)

29. A. G. Evans, S. M. Wiederhorn, J. Mat. Sci. 9 (1974) 1270

30. G. Grathwohl, pp. 573-86 in Deformation of Ceramic Materials II, ed. by R. E. Tressler and R. C. Bradt, Plenum Press, New York, N. Y. (1984)

31. R. C. Folweiler, J. Appl. Phys. 32 (1961) 773

32. W. D. Kingery, H. K. Bowen and D. R. Uhlmann, p. 808 in Introduction to Ceramics, John Wiley and Sons, N. Y. (1976)

33. R. L. Coble, J. Appl. Phys. 34 (1964) 1679

34. T. G. Langdon and F. A. Mohamed, J. Mat. Sci. 13 (1978) 473

35. R. A. Sack, Proc. Phys. Soc. London 58A (1946) 729

36. W. Groebner, N. Hofreiter, Tables of Integrals, Part I, Springer Verlag, New York, N. Y. (1975)

37. A. G. Evans, M. Linzer and L. R. Russell, Mat. Sci. and Eng. 15 (1974) 253

38. T. G. Langdon, Metals Forum 2 (1978) 59

39. J. Weertman, Trans. Amer. Soc. Mat. 62 (1969) 502

40. A. Venkateswaran, D. P. H. Hasselman, J. Mat. Sci. 16 (1981) 1627

41. D. P. H. Hasselman, J. Mat. Sci. 18 (1983) 161

Table 1. Typical Values for Polycrystalline Alumina used for Calculation of Strain-Rate Sensitivity at 1400 ^{o}C

Property or Parameter	Value
Critical Stress Intensity Factor, K_{IC}	2 x 10^{6} $Nm^{-3/2}$
Stress Intensity Exponent, N	10
Constant A in $V = AK_I^N$	10^{-67} MKS units
Young's modulus, E_o	330 GPa
Crack radius, ℓ_o	50μm
Geometric constant, Y	1 .09
Poisson's ratio	0.26

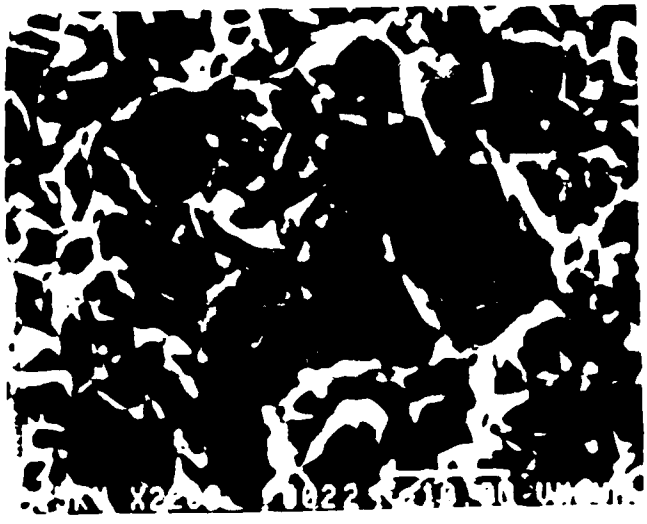

Figure 1. Room temperature SEM-fractograph of 838 alumina.

Figure 2. Scanning electron micrograph of polished section through as-received 838 alumina.

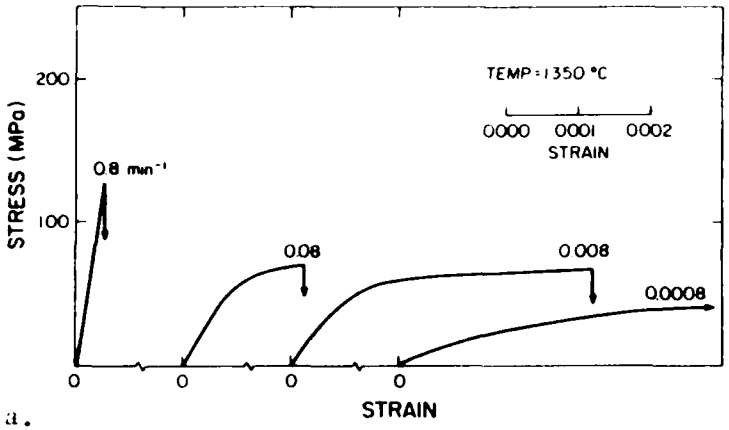

a.

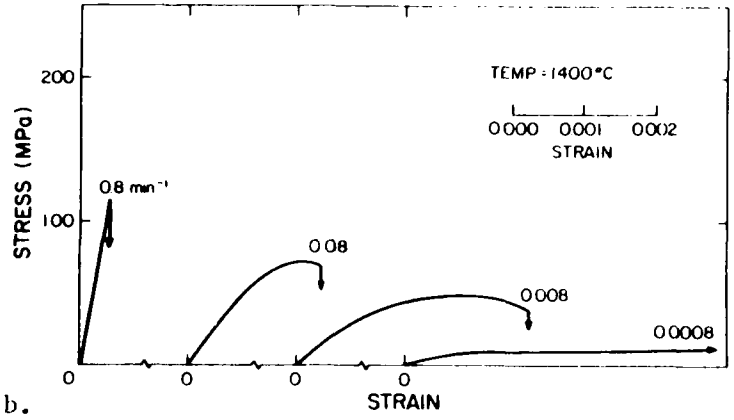

b.

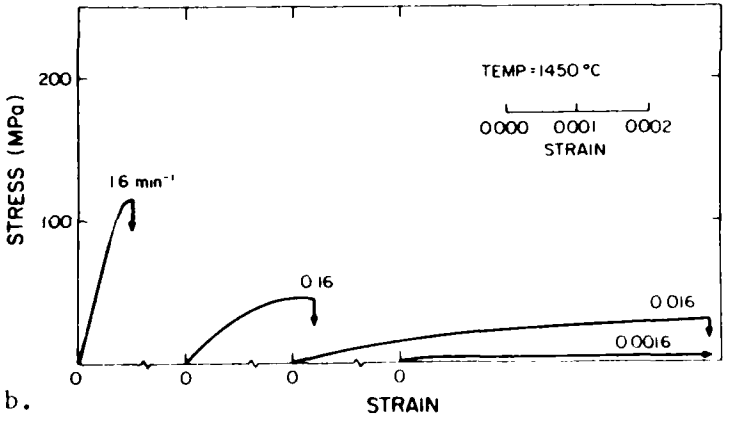

b.

Figure 3. Typical stress-strain response of 838-alumina deformed over range of values of strain rate at: a, 1350; b, 1400 and c, 1450°C.

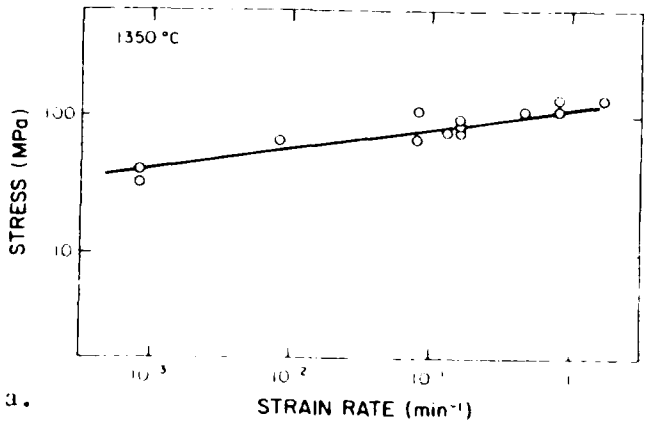

a.

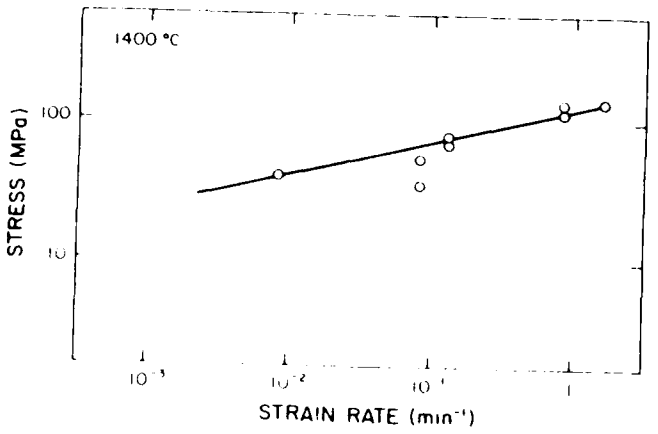

b.

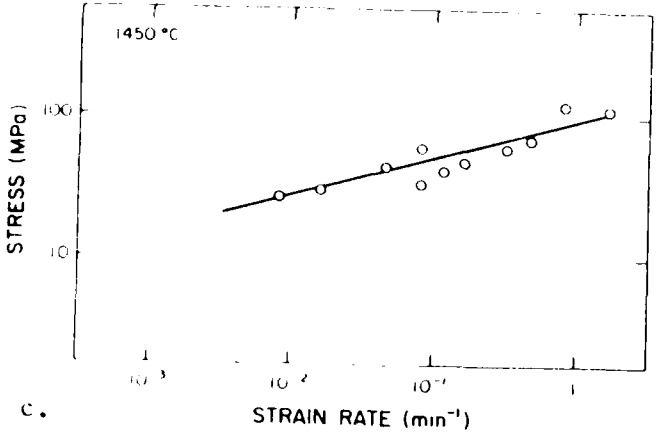

c.

Fig. 4. Dependence of fracture stress of 838-alumina on strain rate at: a, 1350; b, 1400 and c, 1450°C.

a.

b.

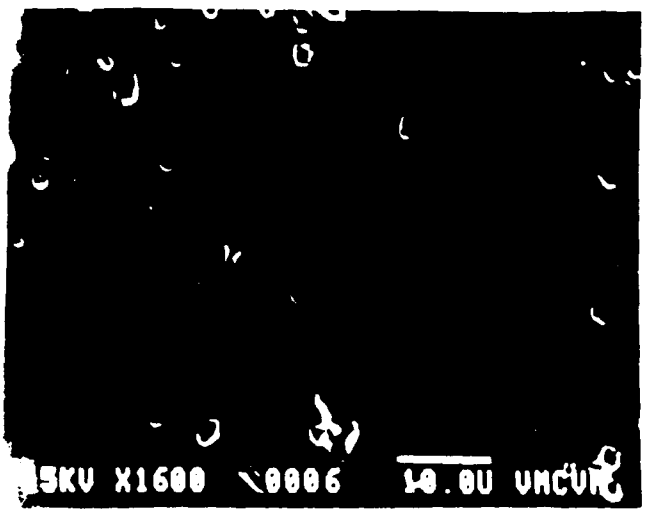

Figure 5. Scanning electron micrographs of polished sections through line of maximum tensile stress at micrograph's right-hand edge of specimens deformed at 1350°C and; a, 0.08 and b, 0.8 min^{-1}.

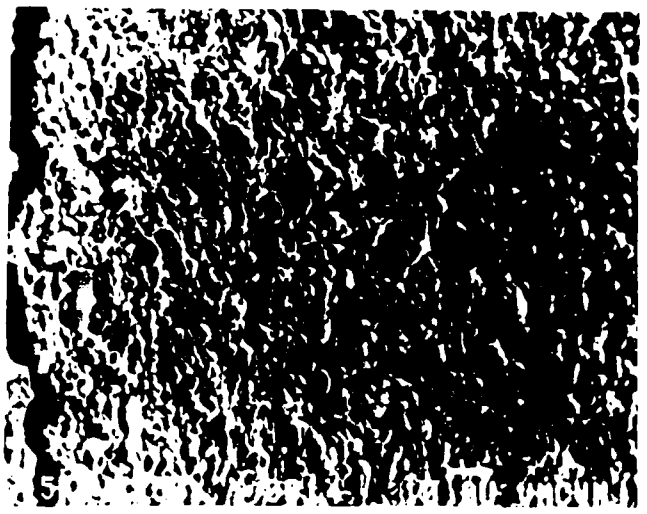

Figure 6. Scanning electron micrograph of tensile surface of specimen deformed at 1350^{o}C and 0.08 min^{-1}.

a.

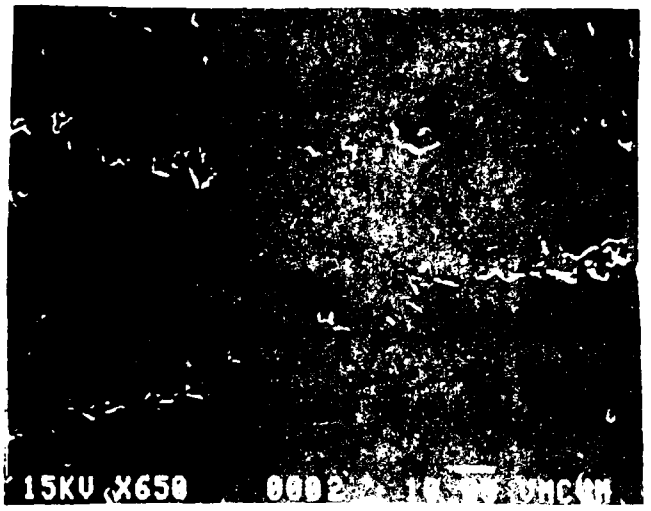

b.

Figure 7. Scanning [illegible] sections through line of maximum [illegible] specimens deformed at 1400°C and [illegible]

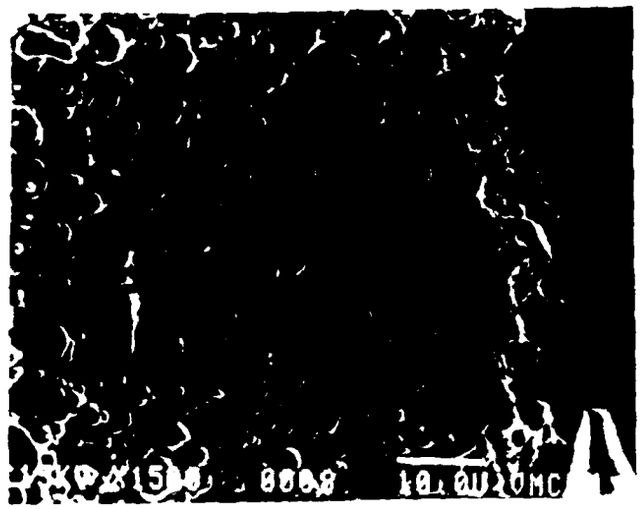

Figure 8. Scanning electron micrograph of tensile surface near fracture plane of specimen deformed at 1400°C and 0.08 min^{-1}.

a.

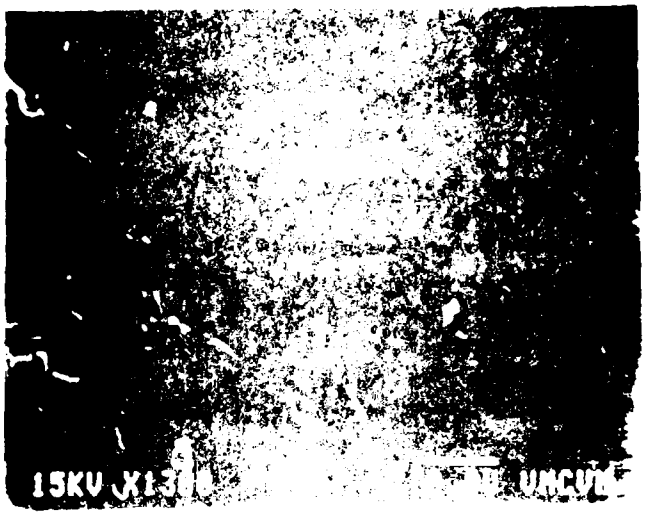

b.

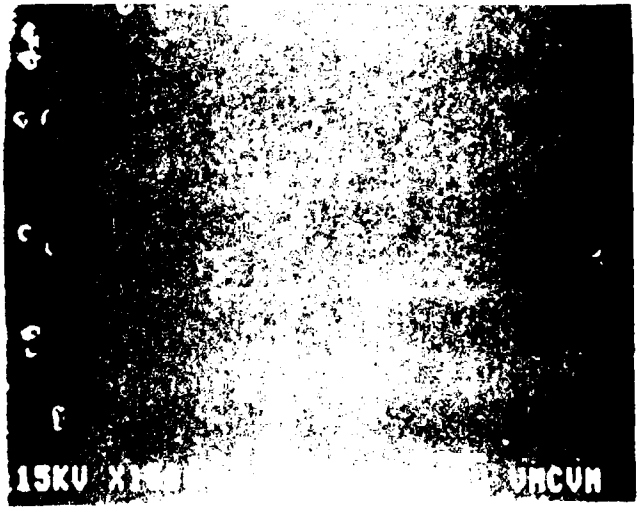

Figure 9. Scanning
of maximum tensile
at 1450°C and a,
ions through line
of specimens deformed

a.

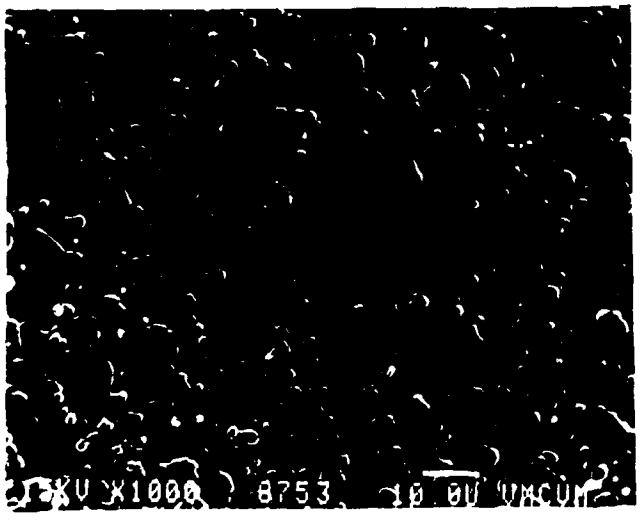

b.

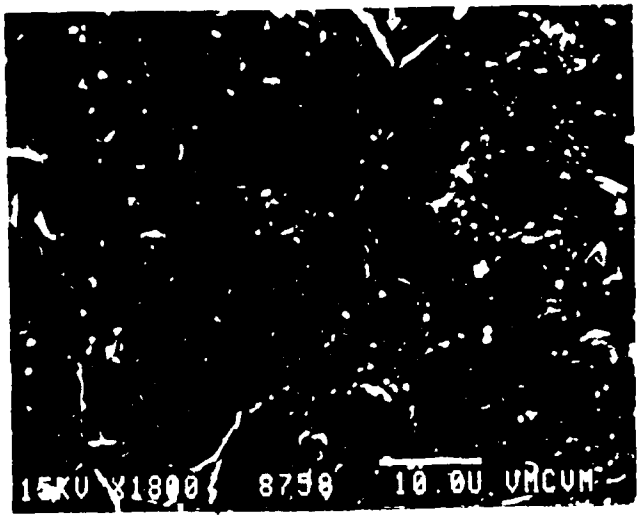

Figure 10. Scanning electron micrographs of tensile surface of specimens deformed at 145°C and a. 0.16 and b. 0.32 min^{-1}.

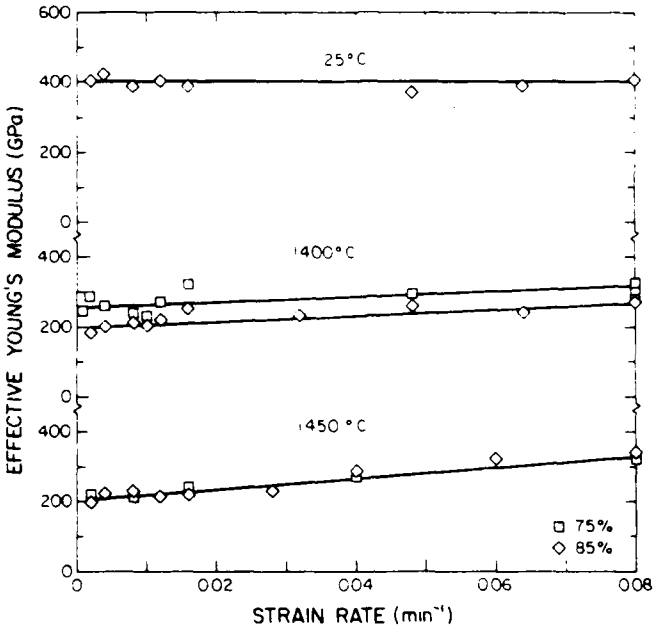

Figure 11. Effective Young's modulus at room temperature following deformation over a range of strain rates to approximately 75 and 85% of the failure strain at 25, 1400 and 1450°C.

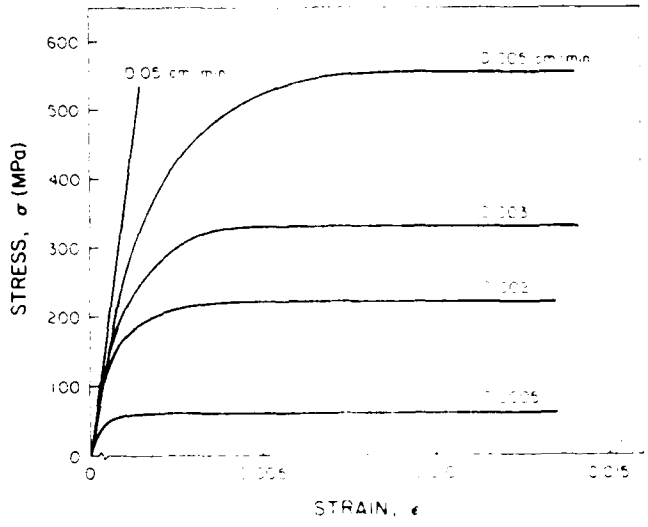

Figure 12. Calculated stress-strain response for non-linear deformation controlled by Coble creep.

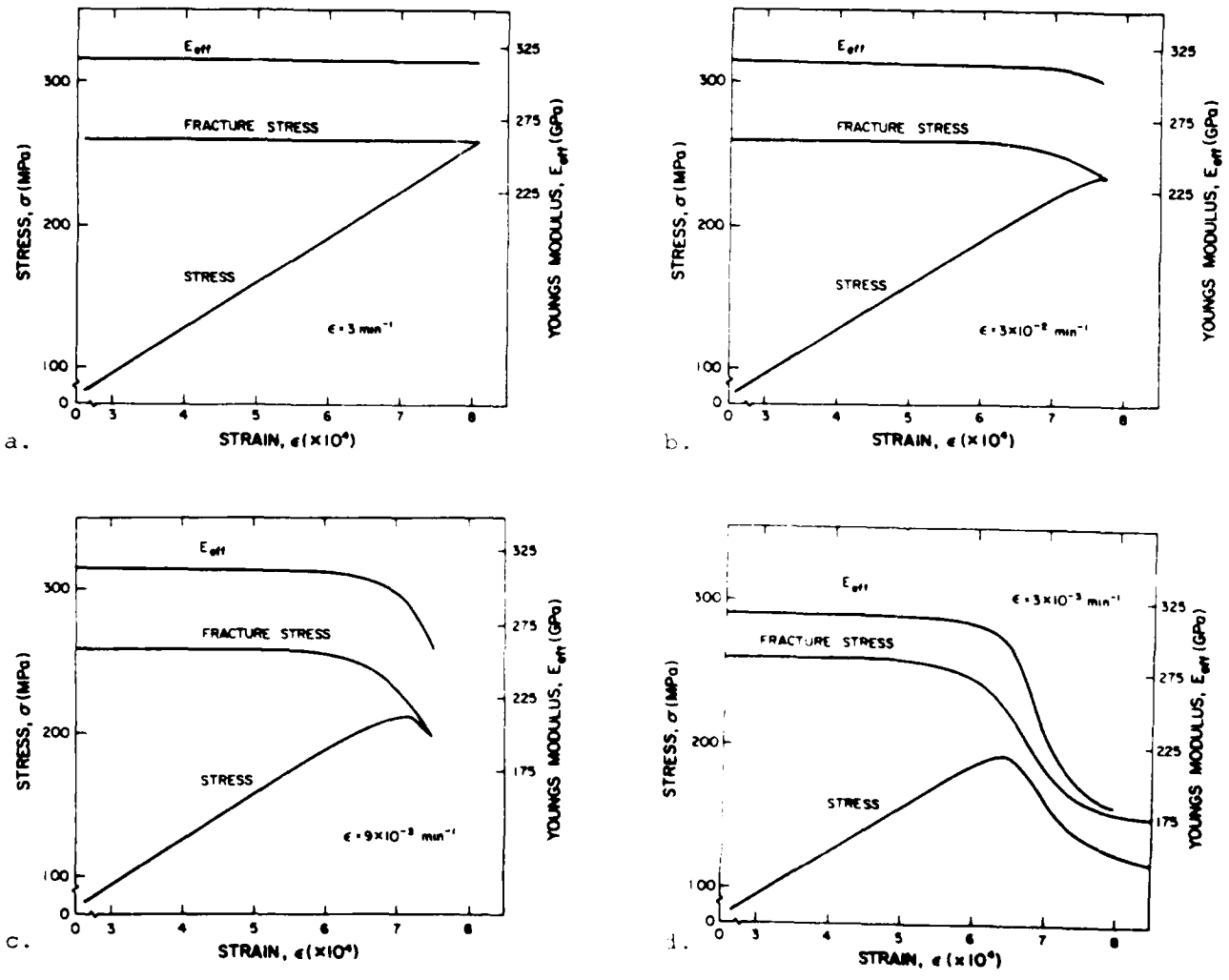

Figure 13. Calculated stress-strain response and change in fracture stress and effective Young's modulus of polycrystalline aluminum oxide simultaneously undergoing Coble creep and multiple sub-critical crack growth for a range of strain-rates.

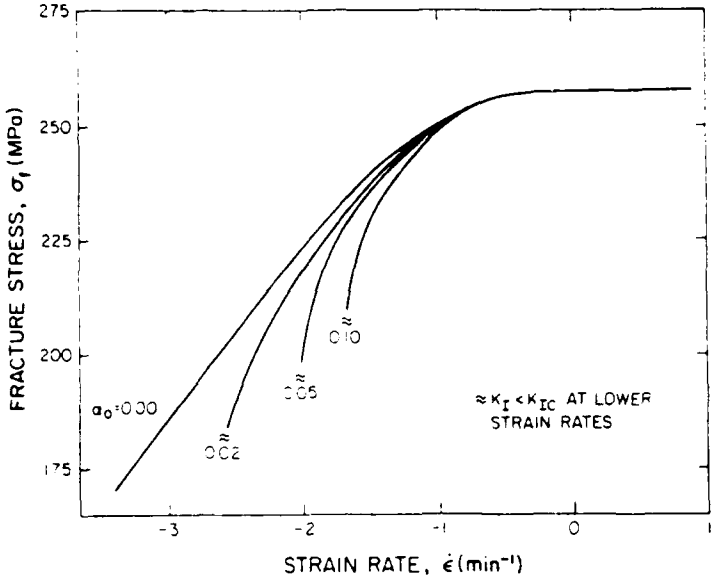

Figure 14. Log-log plot of calculated strain-rate dependence of polycrystalline aluminum oxide undergoing simultaneous deformation by Coble creep and multiple sub-critical crack growth for a range of initial values of a_o in $E_{eff}=E_o\ (1+a_o)^{-1}$.

Role of Intergranular Damage-Induced Decrease in Young's Modulus in the Non-Linear Deformation and Fracture of an Alumina at Elevated Temperatures

A. Venkateswaran, K. Y. Donaldson, D. P. H. Hasselman

Department of Materials Engineering

Virginia Polytechnic Institute and State University

Blacksburg, Va. 24061

ABSTRACT

The effect of the time-dependent decrease in Young's modulus due to damage accumulation by pore growth and intergranular cracking on the stress-strain behavior of a coarse-grained polycrystalline alumina deformed under conditions of displacement-control at elevated temperatures was investigated. Considerable non-linearity in stress-strain behavior, which increased with decreasing strain-rate was noted. At the higher strain-rates, the failure stress was found to be independent of strain-rate, thought to be due to a strain-rate dependent fracture toughness due to the growth of microcracks at the tip of the failure-initiating macrocrack, which offsets the expected strain-rate sensitivity due to the growth of a single macrocrack only. Pore growth and intergranular cracking, accompanied by major reduction in Young's modulus by as much as a factor of five, was most pronounced at the intermediate values of strain rate. This decrease in Young's modulus, under conditions of displacement-controlled loading, results in a decrease in stress, referred to as strain-softening, which contributed to the observed non-linear deformation. This conclusion was confirmed by a theoretical analysis, which showed that in addition to diffusional creep, time-dependent decreases in Young's modulus (elastic creep) by crack growth can make significant contributions to non-linear deformation.

I. INTRODUCTION

Many structural materials when subjected to mechanical loading can exhibit highly non-linear deformation (i.e., inelastic behavior). In ductile metals at ambient temperatures, dislocation motion and multiplication represent the primary mechanisms for non-linear deformation [1-4]. For polycrystalline ceramics at elevated temperatures, non-linear deformation by diffusional creep is a generally well-accepted phenomenon [5-7]. Amorphous materials such as glasses and polymers deform non-linearly by viscous flow [8]. Such viscous flow can constitute the primary mechanism for non-linear deformation in polycrystalline ceramics with a glassy grain boundary phase [9-11]. In general, extensive literature research and analyses have shown that non-linear deformation and its associated dominant mechanism are highly dependent on the stress (or stress-rate) and temperature, as well as on microstructural variables such as grain size and crystallinity and/or the width or composition of a glassy grain boundary phase, if present.

The presence or formation of microcracks is increasingly recognized as a separate effect which can influence the deformation of brittle materials. In geological materials at ambient temperatures, the presence and/or growth of cracks can lead to non-linear stress-strain behavior, creep, dilatancy, stress relaxation and stress-strain behavior which is a function of prior loading history [12-18]. Microcracking in geological materials also can lead to major reductions in elastic moduli [19-21]. During displacement-controlled loading of materials such as rock and concrete, the formation of cracks and subsequent decrease in elastic moduli results in a reduction in measured stress, referred to as "strain-softening" [22-26].

The existence of microcracks in brittle structural ceramics at ambient temperatures is well recognized. They can form during cooling from manufacturing temperatures from internal stresses caused by thermal expansion anisotropy of the grains in polycrystalline ceramics [27] or from the thermal expansion mismatch between the components in brittle matrix composites. Their presence can lead to a major reduction in Young's modulus [28] and to an increase in fracture energy [28], thermal shock resistance [29-31] and thermal insulating ability [32]. Due to subcritical crack growth by stress-corrosion, microcracked materials can exhibit creep at ambient temperatures [33-34]. Stress-induced microcracking can also cause a significant increase in fracture toughness [35].

At elevated temperatures, microcrack formation in polycrystalline structural ceramics under mechanical load can occur as the result of grain-boundary sliding [36] and cavitation [37-39]. Viscous deformation of a glassy grain boundary phase can lead to grain boundary separation followed by crack formation. Since the presence or formation of microcracks can significantly influence the deformation of structural ceramics at ambient temperatures, similar results should be expected at elevated temperatures. Two such separate effects have been identified. The first, due to the transfer of stress from microcracked regions within the material to regions without microcracks, results in an increase in the effective creep rate over the corresponding value found in uncracked materials. This mechanism, labelled "crack-enhanced" creep, was originally formulated by Weertman [40] for Griffith cracks and was extended to penny-shaped cracks for a variety of loading conditions by two of the authors of the present study [41, 42]. The second arises from the formation of new microcracks or

the growth of existing ones, resulting in a corresponding time-dependent decrease in effective elastic moduli. This effect, under an applied stress, gives rise to a time-dependent elastic strain, referred to as "elastic creep" [43].

The concepts of crack-enhanced and elastic creep were used effectively to explain several apparent anomalies in the creep and fracture behavior of structural ceramics, such as the transition from linear to power-law creep in uranium dioxide at levels of temperature and stress far below those predicted from theory, an anomalous grain size dependence of creep rate, discrepancies between diffusion coefficients inferred from creep data and those measured directly, an anomalously high activation energy for creep, the relaxation of residual stresses in polycrystalline aluminum oxide at temperatures ($\sim$ 850 ^{o}C) far below those at which diffusional creep can make a significant contribution and an anomalously high strain-rate sensitivity of the failure stress of a polycrystalline aluminum oxide [44-51].

The phenomena of crack-enhanced creep and elastic creep by crack growth were formulated for conditions of constant applied stress. They could, however, also be the primary mechanisms for non-linear deformation during dynamic loading used to establish stress-strain behavior. The purpose of the present study was to investigate the incidence of crack formation and its effect on subsequent stress-strain behavior of a polycrystalline aluminum oxide subjected to a range of values of constant-rate, displacement-controlled loading.

II. Experimental Details and Theoretical Modelling

A. Material

The sample material chosen for this study was a translucent, coarse-grained polycrystalline aluminum oxide*. Scanning electron micrographs of the external specimen surface, a room temperature fracture surface and a polished section of the specimen interior are shown in figs. 1a, b and c, resp. This alumina is near theoretical density and exhibits an occasional, more or less equi-dimensional pore with an average diameter of a few μm. Grain size ranged from a few μm to as large as 80 μm, with an average value of approx. 38 μm.

Test samples consisted of solid circular rods with a length of ~ 50 mm and a diameter of ~ 6 mm. Prior to testing, all samples were annealed at about 1000 ^{o}C for 6-7 hrs to minimize or eliminate the effect of any residual stresses.

B. Mechanical test procedures

Specimens were tested in 4-point bending with inner and outer spans measuring 10 and 40 mm, resp., using a silicon carbide fixture and carbon pins which were permitted to rotate freely in order to keep extraneous stresses to a minimum. Testing was done in an argon atmosphere within an environmental chamber resistively heated with tungsten mesh heating

---

*Vistal, Coors Porcelain Co., Golden, Colorado

elements. The environmental chamber was contained within the load-frame of an electro- hydraulic closed-loop mechanical tester*. Displacement of the actuator and the resulting load were transferred via water-cooled steel and tungsten push-rods to the specimen and load cell. Metal bellows with rubber seals isolated the furnace atmosphere. Frictional sliding of the seals introduced an uncertainty in the measured load of a few Newtons and an associated uncertainty in the reported stress-strain behavior at the lowest values of stress. Displacement of the actuator was measured using a displacement gauge held against the actuator outside the environmental chamber. This gauge, with a range of ~ 4 mm, permitted measurement of the displacement to ~ 1 μm. By making a separate measurement of the load train's elastic displacement without the specimen, the displacement of the specimen loading points could be obtained by the appropriate subtraction. For the test material and specimen size of this study, the elastic displacement of the specimen and load train were approximately equal in value. Load as a function of time was recorded with an x-y recorder for all values of displacement rate except 1 and 5 cm/min, for which an oscilloscope was used. Although the load at failure could be established accurately at the oscilloscope's lower sweep rate, a higher degree of uncertainty existed in the measurement of displacement.

To establish stress-strain behavior, specimens were loaded over a range of values of displacement rates either to fracture or to a total displacement of ~ 2 mm if fracture did not occur. Preliminary tests showed

---

*MTS Corp., Minneapolis, MN

that temperatures of 1650, 1700 and 1750 ^{o}C were required for non-linear mechanical response over the range of displacement rates used. However, it was found that at 1750 ^{o}C some reaction occurred at the interface between the specimens and carbon pins, introducing some degree of uncertainty in the measurement of displacement. For this reason, most of the data and other supporting evidence to be reported will concentrate on the data obtained at 1650 and 1700 ^{o}C.

The displacement-load data were converted to strain and stress using the theory for pure bending of homogeneous beams [52]. However, as crack formation was found to occur in the tensile stress zone of the specimen, causing a shift in the neutral axis, the use of pure bending theory results in an overestimate of the value of the tensile stress. An analysis of this effect is beyond the scope of the present study, but is underway by others [53].

To measure possible changes in Young's modulus, specimens were deformed at 1650 and 1700 ^{o}C to approx. 75 % of the displacement required to cause fracture, as established in the tests for stress-strain behavior. These specimens were then re-subjected to mechanical loading at room temperature to a load not exceeding 75N, in order to avoid fracture. The effective Young's modulus was then calculated from the load-displacement data, again assuming pure bending behavior.

C. Fractography

External and fracture surfaces of as-received and deformed specimens (if broken) were examined by scanning electron microscopy. Selected

deformed specimens were also sectioned by a low-speed diamond saw and then diamond-polished to provide a cross-section of the specimen interior ranging from the line of maximum tensile stress to the maximum compressive stress. These polished sections were then examined by scanning electron microscopy to reveal the degree of microcracking in the specimen interior. Resulting micrographs were taken such that the line of maximum tensile stress occurred on the right-hand side while the line of maximum compressive stress occurred on the left-hand side.

D. Theoretical Modelling

The stress-strain behavior of a material simultaneously undergoing diffusional creep and elastic creep by microcrack growth was modelled theoretically. The mechanical model selected consisted of a solid with parallel non-interacting penny-shaped cracks subjected to a uniform constant strain rate applied perpendicularly to the crack plane.

The effective Young's modulus perpendicular to the plane of the cracks can be written [31]:

$$E_{eff} = E_o(1 + \alpha_E)^{-1} \tag{1a}$$

where

$$\alpha_E = 16\ (1 - \nu_o^2)\ N_c b^3/3 \tag{1b}$$

in which E_{eff} and E_o are the Young`s moduli with and without cracks, resp., $\nu_o$ is Poisson`s ratio of the crack-free material, N_c is the number of cracks per unit volume and b is the radius of the cracks. For simplicity, the crack density, N_c, will be assumed to be constant, although in practice

N_c is expected to increase with time.

The rate of elastic creep, $\dot{\varepsilon}_E$, due to crack growth can be derived by noting that the elastic strain, ε_E for any value of effective Young's modulus is:

$$\varepsilon_E = \sigma/E_{eff} \tag{2}$$

Upon substitution of eq. 1a, followed by differentiation with respect to time, eq. 2 yields, for constant crack density:

$$\dot{\varepsilon}_E = 16\ (1 - \nu_o^2)\ N_c b^2 \dot{b}/E \tag{3}$$

The dependence of the crack velocity, $\dot{b}$, on the mode I stress intensity factor, K_I, was assumed to be of the form:

$$\dot{b} = db/dt = AK_I^N \tag{4}$$

where A and N are constants.

For a penny-shaped crack the dependence of the stress intensity factor (K_I) on stress (σ) and crack radius (b) can be derived from Sack [54] to be:

$$K_I = 2(1 - \nu_o^2)^{1/2}\ \sigma b^{1/2}/\Pi^{1/2} = \sigma Y b^{1/2} \tag{5}$$

where $Y = 2(1-\nu_o^2)^{1/2}/\Pi^{1/2}$.

The rate of diffusional creep in the absence of cracks ($\dot{\varepsilon}_o$) at any value of instantaneous stress (σ) for the mean grain size of the test material and temperature range of this study was assumed to be controlled by volume-diffusion of the Al^{3+} ion, as described by the Nabarro-Herring theory [5, 6, 55]:

$$\dot{\varepsilon}_o = 20\,\Omega_v(\sigma/d^2)(D_o/KT)\exp(-Q/RT) \tag{6a}$$

where d is the grain size (38 μm for the present study), Ω_v is the molecular volume, D_o is the pre-exponential diffusion constant, Q is the activation

energy, T is the absolute temperature, K is the Boltzmann constant = 1.38 x 10^{-23} J/^{o}K, and R is the gas constant = 8.31 J/mole ^{o}K. For calculations of the diffusional creep rate, appropriate values for Ω_v, D_o and Q were taken from the study of Langdon and Mohamed [55] and are listed in Table I. For any specific temperature, eq. 6a can be written as:

$$\dot{\varepsilon}_o = B\sigma \tag{6b}$$

where $B = 20\Omega_v D_o \exp(-Q/RT)/d^2KT$.

The rate of crack-enhanced linear creep, $\dot{\varepsilon}_c$, for parallel non-interacting penny-shaped cracks is [41]:

$$\dot{\varepsilon}_c = \dot{\varepsilon}_o(1 + \alpha_c) \tag{7a}$$

where α_c is obtained from α_E (eq. 1b) by setting $\nu_o = 0.5$ in order to preserve material volume.

With the aid of eq. 6b, eq. 7a becomes:

$$\dot{\varepsilon}_c = B\sigma(1 + \alpha_c) \tag{7b}$$

Although crack-enhanced creep and elastic creep by crack growth are independent mechanisms, for conditions of mechanical loading with a constant strain rate, they are subject to the constraints:

$$\dot{\varepsilon}_c + \dot{\varepsilon}_E = \dot{\varepsilon}_A \tag{8a}$$

and

$$\int_0^t (\dot{\varepsilon}_c + \dot{\varepsilon}_E)dt = \dot{\varepsilon}_A t \tag{8b}$$

where $\dot{\varepsilon}_A$ is the applied strain rate and t is the time. At time t = 0, it is assumed that the applied strain and the stress in the body equal zero.

In order to predict stress-strain behavior involving elastic deformation, elastic creep by crack growth and crack-enhanced diffusional creep, expressions need to be derived for the elastic strain, diffusional

creep strain and stress as a function of time.

Substituting eq. 1a into eq. 2, differentiating and substituting the results into eq. 8a, and using eq. 7b, yields:

$$\dot{\varepsilon}_E = (1/E_o)d/dt[\sigma(1 + \alpha_E)] = \dot{\varepsilon}_A - B\sigma(1 + \alpha_C) \quad (9)$$

Solution of eq. 9 should yield $\dot{\varepsilon}_E$ as a function of time, from which the variation of $\dot{\varepsilon}_c$, α_E and α_c with time can be obtained with the aid of eqs. 8a and 7b. Unfortunately, an extensive search of the literature and mathematical handbooks was unsuccessful in finding an analytical solution for $\alpha_E \neq \alpha_c$. However, analytical solutions can be derived if the approximation $\alpha_E = \alpha_c$ is made. For aluminum oxide $\nu_o = 0.25$, which yields $\alpha_E = 5N_c b^3$. Since $\alpha_c = 4N_c b^3$ (see eq. 7a), the above approximation yields a conservative estimate of the contribution of elastic creep by crack growth. With the assumption $\alpha_c = \alpha_E = \alpha$, equation 9 can be re-written as:

$$\dot{\varepsilon}_E = 1/E_o d/dt[\sigma(1 + \alpha)] = \dot{\varepsilon}_A - B\sigma(1 + \alpha) \quad (10)$$

which upon re-differentiation yields:

$$-B\ d/dt[\sigma(1 + \alpha)] = 1/E_o\ d^2/dt^2[\sigma(1 + \alpha)] \quad (11)$$

which can be written in integral form, as:

$$f'(t)\ dt/f(t) = -E_o B dt \quad (12)$$

where, for convenience, $f(t) = d/dt[\sigma(1 + \alpha)]$ and $f'(t) = df(t)/dt$.

Integration of equation 12 yields:

$$f(t) = c\exp(-BE_o t) \quad (13)$$

The constant of integration, c, can be evaluated by re-writing eq. 10 in the form:

$$\dot{\varepsilon}_E = (1/E_o)f(t) = \dot{\varepsilon}_A - \dot{\varepsilon}_c \quad (14)$$

At time t = 0, the stress in the body equals zero and therefore $\dot{\varepsilon}_c = 0$. Substitution of $\dot{\varepsilon}_c = 0$ into eq. 14 yields $f(t) = E_o \dot{\varepsilon}_A$, which, when

substituted into equation 13, at t = 0, yields $c = \dot{\varepsilon}_A E_o$. Consequently, eq. 13 can be re-written as:

$$f(t) = \dot{\varepsilon}_A E_o \exp(-BE_o t) \tag{15}$$

Substitution of eq. 15 into eq. 14 yields:

$$\dot{\varepsilon}_E = f(t)/E_o = \dot{\varepsilon}_A \exp(-BE_o t) \tag{16a}$$

which when substituted into eq. 8a yields:

$$\dot{\varepsilon}_c = \dot{\varepsilon}_A (1-\exp(-BE_o t)) \tag{16b}$$

The associated total creep strains can be obtained as:

$$\varepsilon_E = (\dot{\varepsilon}_A/BE_o)[1-\exp(-BE_o t)] \tag{17a}$$

and:

$$\varepsilon_c = \dot{\varepsilon}_A (t - \{(1/BE_o)[1 - \exp(-BE_o t)]\} \tag{17b}$$

The stress, $\sigma(t)$, with the aid of eq. 16b and eq. 7b can be written:

$$\sigma(t) = \dot{\varepsilon}_A [1 - \exp(-BE_o t)]/B(1 + \alpha_E)] \tag{18}$$

where α_E is given by eq. 1b and $\alpha_E = \alpha_E(t)$ because $b = b(\sigma,t)$ and $\sigma = \sigma(t)$.

Substituting eq. 18 into eq. 5, which in turn is substituted into eq. 4, yields:

$$\dot{b} = AY^N b^{N/2} \left[\dot{\varepsilon}_A\{1 - \exp(-BE_o t)\}/B\{1 + 16(1 - \nu_o^2)N_c b^3\}/3\right]^N \tag{19}$$

which can be written in integral form:

$$\int_{b_o}^{b} [\{1 + 16(1 - \nu_o^2)N_c b^3/3\}^N/b^{N/2}]db = (AY^N \dot{\varepsilon}_A^N/B^N) \int_o^t \{1 - \exp(-BE_o t)\}^N dt \tag{20}$$

The left-hand side of eq. 20 can be evaluated with the aid of solutions given by Groebner and Hofreiter [56]. The right-hand integral can be converted to a finite series representation. Unfortunately, these solutions (also used in a prior study [51]) are too complex and lengthy for reproduction here. Time-dependence of the stress was evaluated with the aid of a computer program, where the crack length as a function of time was

evaluated numerically.

Finally, the onset of failure was predicted from the condition:

$$K_I = K_{IC} \tag{21}$$

where K_{IC} is the critical stress intensity factor.

III. Results, Discussion and Conclusions

Figs. 2a, b and c indicate typical stress-strain behavior for selected specimens tested at 1650, 1700 and 1750 ^{o}C, resp., over a range of strain rates. At all three temperatures considerable non-linearity in stress-strain behavior can be noted, with total non-linear strain increasing with decreasing strain rate. Also, in general, at any given value of strain rate, the magnitude of stress reached decreased with increasing temperature. Most specimens exhibited fracture. For those subjected to the lower strain rates, the stress levelled off to a constant value and no failure occurred prior to a displacement of 2mm, indicating that the samples were deforming by creep at a rate equal to the machine displacement rate.

Over the intermediate range of strain rates the non-linear stress-strain behavior in Fig.2 resembles that of work-hardening metallic materials. However, for specimens which retain essentially the same cross-section throughout a test, as did the alumina of this study, work-hardening curves will not show a decrease with increasing strain. This behavior is instead related to microstructural changes accompanying the deformation, as indicated in the following scanning electron micrographs of a series of specimens deformed at 1650 ^{o}C over a range of strain rates.

Fig. 3 shows the surface of a bend-specimen deformed at 0.0011 min^{-1} to a maximum tensile stress of 11 MPa. Comparison with fig. 1a indicates that this surface shows no evidence of microstructural changes. The surface subjected to maximum compressive stress and the polished sections of the specimen interior also revealed no evidence of microstructural changes.

Fig. 4a shows the surface of a specimen deformed at a rate of 0.0033 min^{-1} to a maximum tensile stress of ~12.6 MPa. This surface exhibits more-or-less equidimensionally shaped cavities, located primarily at triple points but occasionally located along grain boundaries. No surface pore formation was found on the maximum compressive stress surface of Fig. 4b. Figs. 4c and d show polished sections taken through the specimen's interior along the lines of maximum tensile and compressive stress, resp. and, when compared with the polished section of the as-received, annealed specimen shown in Fig. 1c, indicate that deformation seems to have been accompanied by the growth of pores perpendicular to the tensile stress and parallel to the compressive stress. Combining this with the fact that equidimensional surface pores were formed, the microstructural evidence seems to indicate that for a specimen deformed at 0.0033 min^{-1}, the stress developed in the specimen is great enough to cause cylindrical cavity formation. The stress reached is not great enough, however, to cause the cavities to become cracks, presumably because of the competition between the diffusional mechanism for crack growth, which tends to increase the cracks' surface area, and localized diffusional processes, which tend to reduce the cracks' surface area.

Fig. 5a shows the surface of a specimen subjected to a maximum tensile stress of ~ 20 MPa at a strain rate of 0.0043 min^{-1}, again at 1650 ^{o}C. This

surface, in contrast to those shown in figs. 3a and 4a, exhibits isolated grain boundary cracks, suggesting that under these test conditions crack nuclei can grow into isolated crack-like cavities. Distances between the cracks appear to be large enough that significant crack-interaction effects and associated crack-linking do not occur.

Fig. 6a shows the tensile surface of a specimen subjected to a maximum tensile stress of ~ 28.4 MPa at a strain rate of 0.0054 min^{-1}. This surface shows a number of isolated grain boundary cracks, similar to those shown in fig. 5a, and an array of more-or-less interconnected inter-granular cracks. Formation of this crack array suggests that for this strain rate the stress developed was high enough that the formation of a single crack could cause crack formation and growth on adjacent grain boundaries. The surface subjected to the maximum compressive stress is shown in fig. 6b, and indicates the formation of more-or-less equidimensional surface pores, similar to those formed in the tensile surface of the specimen shown in fig. 4. Polished sections of the specimen interior indicated the formation of pores or cracks perpendicular to the tensile stress and parallel to the compressive stress, similar to those shown in fig. 5c and d.

For a specimen subjected to a strain rate of 0.0108 min^{-1}, fig. 7 shows the tensile surface subjected to a maximum stress of ~ 31 MPa. This figure shows the only array of interconnected cracks found on the entire specimen surface. In other areas only a few isolated intergranular cracks and equidimensional cavities could be detected. Neither the specimen surface subjected to compression nor the specimen interior showed any changes in microstructure. Also, for specimens deformed at still higher

strain rates of 0.217 and 1.08 min^{-1} with associated maximum values of tensile stress of 35 and 38 MPa, no microstructural changes could be found in either the external tensile or compressive surface or in the specimen interior.

At 1700 and 1750 ^{o}C, the microstructural changes which accompanied deformation over the total range of strain rates were found to be similar to those which occurred at 1650 ^{o}C. It appeared, however, that at 1700 and 1750 ^{o}C the suppression of cavitation and microcracking at the higher strain rates was shifted to somewhat lower rates.

In general, the microstructural evidence suggests that cavitation and intergranular crack formation are most extensive over the intermediate strain rates and are absent at the lowest and highest strain rates. Qualitatively, such behavior is expected to arise for two reasons. At the lowest rates, the specimens can deform entirely under the influence of diffusional or dislocation creep or grain boundary sliding at a rate sufficient to accommodate the rate of displacement of the mechanical tester, but at a stress level below the minimum value required to cause microstructural changes such as pore growth or intergranular crack formation. At the intermediate rates, the stress rises to values well in excess of the minimum required to cause extensive cavitation. At the highest rates, the time period till failure by the propagation of a single macrocrack is too short to allow observable changes in pore or crack morphology.

Figs. 8a and b show the data for the effective Young's modulus at room temperature as a function of strain rate for samples deformed to approx. 75 % of the fracture strain at 1650 and 1700 ^{o}C, resp. For both temperatures,

a substantial decrease in effective Young's modulus is indicated, especially at the intermediate strain rates. Particularly encouraging from the perspective of the original objective of this study is not only that Young's modulus is decreased substantially, but that these decreases are a maximum over the range of strain-rates where the most microstructural damage was found. It is speculated that if these specimens had been deformed to fracture, the decrease in Young's modulus possibly would have been even greater than indicated by the experimental data. Considering that these data reflect the effective Young's modulus of the deformed specimens as a whole, Young's modulus of the cracked tensile zone is expected to fall well below the data shown in fig. 8.

Figs. 9a and b show the tensile surface and polished section of a specimen deformed at 1650°C at a strain rate of 0.0043 min^{-1}. This specimen corresponds to the minimum in the effective Young's modulus data and exhibits extensive crack formation. The reduction in effective Young's modulus apparent in Fig. 8, however, seems greater than expected from the microstructural evidence shown in fig. 9. Scanning electron microscopy may not reveal all the damage which was created, such as grain boundary cracks that are too narrow to be resolved. The reduction in Young's modulus appears to be governed by a second effect as well. It was observed that a simple anneal for 10 min also caused some decrease in Young's modulus. As indicated by fig. 8, this was most pronounced at 1700 °C. Scanning electron microscopy did not reveal the reason for this decrease. Possibly it is related to microcrack formation in the absence of a load or cavitation due to internal pressure within the pores, as observed by Robertson and Wilkinson [57].

The experimental data for the effective Young's modulus permit making a semi-quantitative estimate of the role of crack formation in the observed non-linear deformation (i.e., the reduction in stress at any given strain compared to entirely elastic behavior in the absence of cracks). As an example, we can focus on the specimen deformed at 1700°C at a strain rate of 0.0054 min^{-1}. For this sample, deformed to a strain of 0.02 (approx. 75% of the failure strain), the effective Young's modulus at room temperature was measured to be ~85 GPa, compared to a value of ~390 GPa for the as-received material. At 1700°C these values are estimated to be reduced by some 10%, i.e., 75 and 350 GPa, resp. This reduction in Young's modulus by a factor of about 4 1/2 causes a corresponding reduction in stress, compared to the elastic behavior without crack formation, from approx. 7,000 to 1,500 MPa. The further reduction in stress must be attributed to some mechanism of diffusional creep. The associated rate of creep deformation due to the presence of cracks is enhanced by a factor about equal to the relative reduction in Young's modulus as indicated by the appropriate analytical expressions presented earlier. This enhancement in creep rate as the cracks form during loading contributes further to the non-linearity of the stress-strain behavior. These effects may well be much larger just prior to failure where Young's modulus may well be reduced by a factor of ten, accompanied by a corresponding increase in creep rate especially for those specimens with stress-strain curves which exhibit a decrease in stress with increasing strain. For equal contributions of the reduction of Young's modulus and the enhancement of creep rate, their combined effects could reduce the stress, compared to entirely elastic behavior without cracks, by as much as two orders of magnitude.

An interesting observation incidental to the primary objective of this study was made in regard to the strain rate sensitivity of the fracture stress, shown in figs. 10a, b and c for the three test temperatures of 1650, 1700 and 1750 ^{o}C, resp. The strain rate sensitivity appears to indicate the existence of a bi-modal dependence. This is particularly noticeable for data obtained at 1750 ^{o}C, which are characterized by an unusually high strain-rate sensitivity at the lower strain rates which resulted in fracture, and strain-rate independent fracture at the higher strain rates. As shown analytically in a prior study [51], such an unusually high strain-rate dependence can be attributed to the strain-rate dependent formation of multiple cracks in addition to the failure-causing macrocrack. This effect results in a decrease in Young's modulus which is an inverse function of the strain rate. The resulting strain-rate dependent strain-softening under conditions of displacement rate-controlled loading in turn is responsible for the high strain-rate sensitivity of the failure stress.

The absence of any significant strain-rate sensitivity of the failure stress at the higher values of strain rate for all three test temperatures appears puzzling. Because of the formation and growth of cracks over this range of strain rates, except at the highest values, some degree of strain-rate sensitivity would be expected as the combined result of sub-critical growth of the failure-causing macrocrack and strain-rate dependent strain-softening due to pore growth and/or grain boundary cracking. It is speculated that these two mechanisms are offset by a third, resulting in no net strain-rate sensitivity of the failure stress. The source of this third postulated mechanism relates to the observed

intergranular microcracking. If such microcracks can form under the influence of the nominal stress field, they are sure to form in the highly stressed regions near the tip of the macrocrack responsible for failure. Microcracking at the tip of a macrocrack will result in an increase in fracture toughness due to stress-induced microcrack toughening [35]. The effectiveness of this latter mechanism will be a function of the degree (i. e., the density and size) of microcrack formation at the macrocrack tip. As indicated by the fractographic information shown in figs 3 through 7, the degree of microcracking will be a function of strain rate, with a greater degree of microcracking occurring at the intermediate values than at the highest values. If indeed the proposed mechanism of stress-induced microcrack toughening is operative, a higher fracture toughness is anticipated in those specimens subjected to the intermediate values of strain rate. In other words, the fracture toughness and associated fracture stress would show an inverse dependence on strain rate. It is suggested that this decrease in fracture stress with increasing strain rate will approximately compensate for the expected increase in fracture stress due to the combined effects of strain-softening in the specimen as a whole, and sub-critical growth of the failure-initiating macrocrack. The verification of the mechanism of strain-rate dependent microcrack toughening is intended to be the subject of a future investigation.

Results for the theoretical modelling of the stress-strain behavior qualitatively reflected the experimental behavior. Table 1 lists the various material property values and other parameters selected for the calculated stress strain behavior. A number of the values and parameters listed represent actual data reported in the literature [55,

AD-A191 405 ROLE OF CRACKS IN THE CREEP OF STRUCTURAL POLYCRYSTALLINE CERAMICS..(U) VIRGINIA POLYTECHNIC INST AND STATE UNIV BLACKSBURG DEPT OF M.. 2/2

UNCLASSIFIED D P HASSELMAN ET AL. 15 JAN 88 F/G 11/2 NL

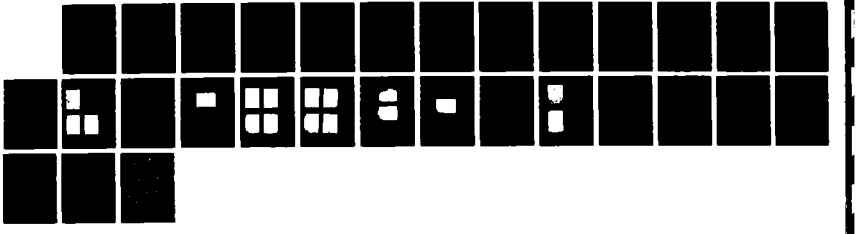

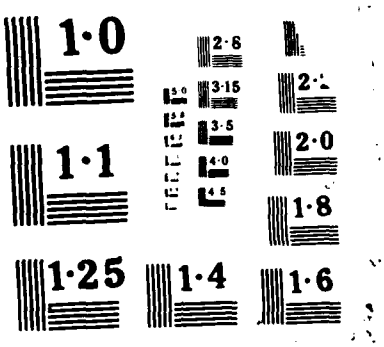
1·0
1·1
1·25
1·4
1·6
2·0
1·8

58]. Others represent reasonable estimates obtained by extrapolation of experimental data at lower temperatures to 1700 ^{o}C [59, 60]. No special assumption was made for the existence of a failure-initiating macrocrack. For the criterion $K_I = K_{IC}$, failure was assumed to occur by the simultaneous propagation of any one of the equally-sized intergranular cracks. The temperature dependence of Young's modulus was calculated from corresponding data for the shear modulus [61]. The values of initial crack size and crack density resulted in an initial value of Young's modulus equal to approx. 99 % of the value for theoretically dense, crack-free aluminum oxide.

Figs. 11a, b, c, d and e show the predicted stress-strain behavior and associated changes in fracture stress and Young's modulus of elasticity for strain rates, $\dot{\varepsilon}_A$ = 300, 30, 18, 3 and 3 x 10^{-8} min^{-1}. Qualitatively, the predicted stress-strain behavior exhibits the same features as the observed behavior shown in fig. 2. At the highest strain rate, the stress-strain curve shows only a slight deviation from linearity and a correspondingly small decrease in fracture stress and Young`s modulus. The degree of non-linearity of the stress-strain curves increases with decreasing strain rate. At the lowest strain rate, as strain increases, the stress-strain curve levels off to a nearly constant value with no decrease in fracture stress and Young's modulus. At this value of strain rate and its associated stress level, the rate of diffusional creep is sufficiently high to completely accommodate the applied strain rate.

At the strain rates of 18 and 3 min^{-1}, the stress-strain curves exhibit a decrease in stress with increasing strain, prior to fracture, an effect also exhibited by a number of the experimental stress-strain curves. At

18 min^{-1}, the stress-strain curve just intersects the fracture stress curve, so that fracture will occur. In contrast, at 3 min^{-1}, the calculated results indicate that the stress at any value of strain is always less than the fracture stress, so that no fracture will occur. Crack growth will take place in a sub-critically stable mode over the total range of deformation.

A quantitative comparison between the experimental stress-strain curves in fig. 2 and the predicted curves shown in fig. 11 indicates that similar stress-strain curves are obtained at strain rates differing by approximately one and a half orders of magnitude. This discrepancy should not be attributed to the incorrectness of the mechanical model, but to the relatively large uncertainty in the magnitude of many of the parameters listed in Table 1. Even minor changes in these values, especially those which affect diffusion and sub-critical crack growth, can have a major effect on the corresponding rates of diffusional creep and creep by crack growth. In principle, by the appropriate adjustment of the magnitude of the pertinent variables, any degree of quantitative agreement between the observed and calculated stress-strain curves can be obtained. This, however, would constitute a curve-fitting exercise of questionable scientific or technical merit. The simplifying assumptions of equal grain size, equal initial crack size and constant crack density and the absence of crack interaction also may have contributed to the differences in equivalent observed and calculated behavior. However, the substantial decrease in Young's modulus following deformation supports the model's general validity.

As pointed out earlier, the stress-strain curves of fig. 11 reflect the

combined effects of diffusional creep and elastic creep by crack growth. It is of interest to explore the relative contributions of these two effects, especially in view of the experimental data on the changes in Young's modulus. As a specific example, stress-strain curves were calculated for deformation by diffusional creep without and with accompanying creep by subcritical crack growth for the very low value of creep rate of 3×10^{-6} min^{-1}, using the values listed in Table 1. These results are shown in figs. 12a and b, resp. In the absence of creep by crack growth, the stress levels off to a constant value of near 3.8 MPa. In contrast, when creep by crack growth is included in the analysis, the stress reaches a peak of only about 6×10^{-1} MPa and then decreases to about 2.5×10^{-1} MPa, indicative of the significant effect of strain-softening by crack formation.

Fig. 13 shows the relative contributions of diffusional and elastic creep to the total creep strain at the instant of fracture or maximum stress in the absence of fracture for a grain size of 38 μm. Similar calculations were also made for various other grain sizes. Fig. 14 is a plot of strain rate at the crossover point, representing equal contributions from elastic creep and crack-enhanced diffusional creep to the total creep strain at σ max or σ fracture, as a function of grain size. In general, the results indicate that elastic creep by crack growth can make a significant contribution to the total strain, especially at the larger values of grain size, where the contribution of diffusional creep, in view of its inverse grain-size dependence, becomes largely suppressed. In fact, at a grain size of 100 μm, the contribution of diffusional creep to the total creep strain was found to approach 100 % only at a strain rate of 10^{-12} min^{-1}. As stated earlier, even minor changes in such parameters

as initial crack size, stress intensity exponent, or activation energy for creep can result in major changes in the corresponding rates of creep by diffusion and crack growth. For this reason, a quantitative comparison between the analytical and experimental results should be treated with caution.

An analysis of the combined effects of creep and crack growth in bending would be highly desirable to aid in the interpretation of this study's results. Such an analysis is expected to be handicapped by a number of complicating variables such as crack formation in the tensile stress zone of the specimen, coupled with a corresponding shift in the location of the neutral axis. Furthermore, spatial variations in Young's modulus within the tensile stress zone are expected. If crossections are assumed to remain plane, crack growth in various positions relative to the neutral axis is expected to be constrained. For this reason, crack formation and associated elastic creep and crack-enhanced creep in the tensile stress zone cannot occur without corresponding enhancement of creep within the compressive zone. Therefore, the different deformation mechanisms in the tensile and compressive zones are expected to be coupled. Such an analysis, which may require step-wise integration, is beyond the scope of the present program.

In summary, the experimental results of this study, supported by theoretical modelling, indicate the significant role crack formation can play in the deformational characteristics of structural ceramics at elevated temperature. Not only should crack formation affect high-temperature behavior for the mechanical loading conditions chosen for this study, but it should also be a factor in deformation due to other loading

conditions, such as constant or cyclic loading. A microstructural analysis of materials following deformation in order to establish the degree of crack formation is judged to be essential for the proper interpretation of deformational behavior of structural ceramics at elevated temperatures.

Acknowledgment

This study was supported by the Army Research Office under Contract No.: DAAG 29-85-K-0106.

Table 1. Values for Material Parameters and External Variables for Theoretical Modelling.

Molecular volume, Ω_v	4.2×10^{-29}	m^3
Diffusion coefficient, D_o	28×10^{-4}	$m^2 s^{-1}$
Activation energy, Q	478	KJ/mole
Grain size, d	38	μm
Temperature, T	1700	^oC
Initial crack size, b_o	3	μm
Stress intensity exponent, N	3	
Constant in $V = AK_I^N$, A	10^{-16}	SI units
Crack density, N_c	6×10^{13}	m^{-3}
Critical stress intensity factor, K_{IC}	0.1	$MN.m^{-3/2}$
Poisson's ratio, ν_o	0.26	
Young's modulus, E_o	319	GPa

References

1. A. H. Cottrell, Dislocations and Plastic Flow in Crystals, Oxford, Clarendon Press, 1956
2. G. E. Dieter, Mechanical Metallurgy, 2nd. Ed., McGraw Hill, Inc. (1976)
3. W. D. Kingery, H. K. Bowen and D. R. Uhlmann, Introduction to Ceramics, 2nd Ed., Wiley, N. Y. (1976)
4. J. Weertman, "Dislocation Climb Theory of Steady-State Creep," Am. Soc. of Met. Transactions 61, 681-93 (1968)
5. F. R. N. Nabarro, "Deformation of Crystals by the Motion of Single Ions," Report on a Conference on Strength of Solids, The Physical Society, London, 75 (1948)
6. C. Herring, "Diffusional Viscocity of a Polycrystalline Solid," J. Appl. Phys. 21, 437 (1950)
7. R. L. Coble, "A Model for Boundary Diffusion Controlled Creep in Polycrystalline Materials," J. Appl. Phys. 34, 1679-1684 (1964)
8. H. S. Y. Hsich, "Physical and Thermodynamic Aspects of the Glassy State and Intrinsic Non-Linear Behavior of Creep and Stress Relaxation," J. Mat. Sci. 15, 1194-1206 (1980)
9. R. Morrell and K. H. G. Ashbee, "High Temperature Creep of Lithium Zinc Silicate Glass-Ceramics," J. Mat. Sci. 8, 1253-1270 (1973)
10. R. Kossowsky, D. G. Miller and E. S. Diaz, "Tensile and Creep Strengths of Hot-Pressed Si_3N_4," J. Mat. Sci. 10, 983-997 (1975)
11. F. F. Lange, "Non-Elastic Deformation of Polycrystals with a Liquid Boundary Phase," pp. 361-81 in Deformation of Ceramic Materials, Eds. R. C. Bradt and R. E. Tressler, Plenum Press, N. Y. (1975)
12. W. F. Brace and E. G. Bombolakis, "A Note on Brittle Crack Growth in

Compression," J. Geophysical Res. 68 (12) 3709-13 (1963)

13. N. G. W. Cook and K. Hodgson, "Some Detailed Stress-Strain Curves for Rock," J. Geophysical Res. 70 (12) 2833-88 (1965)

14. W. G. Brace, B. W. Paulding, Jr. and C. Scholz, "Dilatancy in the Fracture of Crystalline Rocks," J. Geophysical Res. 71 (16) 3939-53 (1966)

15. C. H. Scholz, "Experimental Study of the Fracturing Process in Brittle Rock," J. Geophysical Res. 73 (4) 1947-54 (1968)

16. C. H. Scholz, "Mechanism of Creep in Brittle Rock," J. Geophysical Res. 73 (10) 3295-3302 (1968)

17. D. J. Holcomb, "Memory, Relaxation and Microfracturing in Dilatant Rock," J. Geophysical Res. 86 (B7) 6235-48 (1981)

18. P. L. Swanson, "A Fracture Mechanics and Non-Destructive Evaluation Investigation of the Subcritical-Fracture Process in Rock," pp. 299-318 in Fracture Mechanics of Ceramics, Vol. 8, Ed. by R. C. Bradt, A. G. Evans, D. P. H. Hasselman and F. F. Lange, Plenum Press (1986)

19. J. B. Walsh, "Effect of Cracks on the Compressibility of Rocks," J. Geophys. Res. 70 (2) 381-89 (1965)

20. R. L. Salganik, "Mechanics of Bodies with Many Cracks," Izv. Akad. Nauk. SSR, Mekh. Tverd. Tela. 8, 149-158 (1973)

21. B. Budiansky and R. J. O'Connell, "Elastic Moduli of a Cracked Solid," Int. J. Solid Struct. 12, 81-97 (1976)

22. S. K. Ghosh and M. Z. Cohn, "Non-Linear Analysis of Strain-Softening Structures," pp. 315-332 in Inelasticity and Non-Linearity in Structural Concrete, Ed. by M. Z. Cohn, University of Waterloo Press, Waterloo (1973)

23. G. Maier, A. Zavelani and J. Dotreppe, "Equilibrium Branching Due to Flexural Softening," J. Eng. Mech. Div., ASCE, 99 (EM 4) 897-901 (1973)

24. Z. P. Bazant, "Instability, Ductility, and Size-Effect in Strain-Softening Concrete," J. Eng. Mech. Div., ASCE, 102 (E 2) 331-344 (1976)

25. Z. P. Bazant and B. H. Oh, "Rock Fracture via Strain-Softening Finite Elements," J. Eng. Mech. Div., ASCE, 110 (7) 1015-1035 (1984)

26. E. P. Chen and L. M. Taylor, "Fracture of Brittle Rock Under Dynamic Loading Conditions," pp. 175-86 in Fracture Mechanics of Ceramics, Vol. 7, Ed. by R. C. Bradt, A. G. Evans, D. P. H. Hasselman and F. F. Lange, Plenum Press (1986)

27. A. G. Evans, "Microfracture from Thermal Expansion Anisotropy - I, Single Phase Systems," Acta Metall. 26, 1845-53 (1978)

28. J. A. Kuszyk and R. C. Bradt, "Influence of Grain Size on Effects of Thermal Expansion Anisotropy in $MgTi_2O_5$," J. Amer. Ceram. Soc. 56 (8) 429-33 (1973)

29. D. P. H. Hasselman, "Unified Theory of Thermal Shock Fracture Initiation and Crack Propagation in Brittle Ceramics," J. Amer. Ceram. Soc. 52 (11) 600-04 (1969)

30. R. C. Rossi, "Thermal-Shock-Resistant Ceramic Composites," Amer. Ceram. Soc. Bull. 48 (7) 736-37 (1969)

31. D. P. H. Hasselman and J. P. Singh, "Analysis of Thermal Stress Resistance of Microcracked Brittle Ceramics," Amer. Ceram. Soc. Bull. 58 (9) 856-60 (1979)

32. D. P. H. Hasselman, "Effects of Cracks on Thermal Conductivity," J. Comp. Mater. 12 (10) 403-407 (1978)

33. E. A. Bush and F. A. Hummel, "High-Temperature Mechanical Properties of Ceramic Materials: I," J. Amer. Ceram. Soc. 41 (6) 189-95 (1958); "II", ibid. 42 (8) 388-91 (1959)

34. D. P. H. Hasselman, "Crack Growth and Creep in Brittle Ceramics," J. Amer. Ceram. Soc. 52 (9) 517-18 (1969)

35. Y. Fu and A. G. Evans, "Microcrack Zone Formation in Single Phase Polycrystals," Acta Metall. 30, 1619-25 (1982)

36. A. G. Evans, "Deformation and Failure Caused by Grain Boundary Sliding and Brittle Cracking," Acta Metall. 28, 1155-64 (1980)

37. T. J. Chuang, K. I. Kagawa, J. R. Rice and L. B. Sills, "Non-Equilibrium Models for Diffusive Cavitation of Grain Interfaces," Acta Metall. 27, 265-84 (1979)

38. T. J. Chuang, "A Diffusive Crack-Growth Model for Creep Fracture," J. Amer. Ceram. Soc. 65, 93-103 (1982)

39. A. H. Chokshi and J. R. Porter, "Cavity Development During Creep Deformation in Alumina with a Bimodal Grain Size Distribution," J. Amer. Ceram. Soc. 70 (3) 197-202 (1987)

40. J. Weertman, "Effect of Cracks on Creep Rate," Trans. Amer. Soc. Met. 62, 502-511 (1969)

41. D. P. H. Hasselman and A. Venkateswaran, "Role of Cracks in the Creep Deformation of Brittle Polycrystalline Ceramics," J. Mat. Sci. 18, 161-172 (1983)

42. A. Venkateswaran and D. P. H. Hasselman, "Matrix Representation of the Crack-Enhanced Creep of Ceramics under Conditions of Multi-Axial Loading," pp. 349-56 in Fracture Mechanics of Ceramics, Vol. 7, Ed. by R. C. Bradt, A. G. Evans, D. P. H. Hasselman and F. F. Lange, Plenum

Press, N. Y. (1986)

43. A. Venkateswaran and D. P. H. Hasselman, "Elastic Creep of Stressed Solids Due to Time-Dependent Changes in Elastic Properties," J. Mat. Sci. 16, 1627-1632 (1981)

44. D. P. H. Hasselman and A. Venkateswaran, "Effect of Cracks on Mechanisms and Kinetics of Creep Defornation of Brittle Materials," pp. 525-45 in Deformation of Ceramic Materials II, Ed. by R. E. Tressler and R. C. Bradt, Plenum Press (1984)

45. J. B. Ainscough, F. Rigby and S. A. Morrow, "Effect of Oxygen Potential on the Thermal Creep of Niobia-Doped UO_2," J. Amer. Ceram. Soc. 64 (5) 315-18 (1981)

46. B. Burton, G. L. Reynolds and J. P. Barnes, "The Influence of Grain Size on the Creep of Uranium Dioxide," J. Mat. Sci. 8, 1690-94 (1973)

47. A. Venkateswaran and D. P. H. Hasselman, "Creep Analysis of Bend Specimens Subject to Tensile Cracking," J. Amer. Ceram. Soc. 67 (7) C-144 (1984)

48. R. C. Folweiler, "Creep Behavior of Pore-Free Polycrystalline Aluminum Oxide," J. Appl. Phys. 32 (5) 773-78 (1961)

49. S. I. Warshaw and F. H. Norton, "Deformation Behavior of Polycrystalline Aluminum Oxide," J. Amer. Ceram. Soc. 45, 479-86 (1962)

50. Y. Tree, A. Venkateswaran and D. P. H. Hasselman, "Observations on the Fracture and Deformation Behavior During Annealing of Residually Polycrystalline Aluminum Oxides," J. Mat. Sci. 18, 2135-48 (1983)

51. D. P. H. Hasselman, A. Venkateswaran and K. Y. Donaldson, "Contribution of Damage by Multiple Crack Growth to the Strain-Rate Sensitivity of a Polycrystalline Alumina at Elevated Temperature," J. Mat. Sci. (in

review)

52. S. Timoshenko, Strength of Materials Part I, Van Nostrand, N.Y. (1930)

53. C. F. Chen and T.-J. Chuang, "Microstructural Effects on the Creep Behavior of Sialon Ceramics, II. Presented at 11th Annual Conference on Composites and Advanced Ceramic Materials, Cocoa Beach, Fla. Jan. 18-23, 1987

54. R. A. Sack, "Extension of Griffith's Theory of Rupture to Three Dimensions", Proc. Phys. Soc., London. Sect. A, 58, 729-36 (1946)

55. T. G. Langdon and F. A. Mohamed, "The Incorporation of Ambipolar Diffusion in Deformation Mechanism Maps for Ceramics," J. Mat. Sci. 13, 473-482 (1978)

56. W. Groebner and N. Hofreiter, Table of Integrals, Vol. 1, Indefinite Integrals, Springer Verlag, N. Y. (1975)

57. A. G. Robertson, D. S. Wilkinson, "Damage Accumulation in Hot-Pressed Alumina During Flexural Creep and Anneals in Air," pp. 311-26 in Fracture Mechanics of Ceramics, Vol. 7. Ed. by R. C. Bradt, A. G. Evans, D. P. H. Hasselman and F. F. Lange, Plenum Press (1977)

58. A. E. Paladino and W. D. Kingery, "Aluminum Ion Diffusion in Aluminum Oxide," J. Chem. Phys. 37, 957 (1962)

59. K. Jakus, T. Service and J. E. Ritter, Jr., "High-Temperature Fatigue Behavior of Polycrystalline Alumina," J. Amer. Ceram. Soc. 63 [1] 4-7 (1980)

60. A. G. Evans, M. Linzer and L. R. Russell, "Acoustic Emission and Crack Propagation in Polycrystalline Alumina," Mat. Sci. and Eng. 15, 253-61 (1974)

61. T. G. Langdon, "Recent Developments in Deformation Mechanism Maps," Metals Forum, 1, 59-70 (1978)

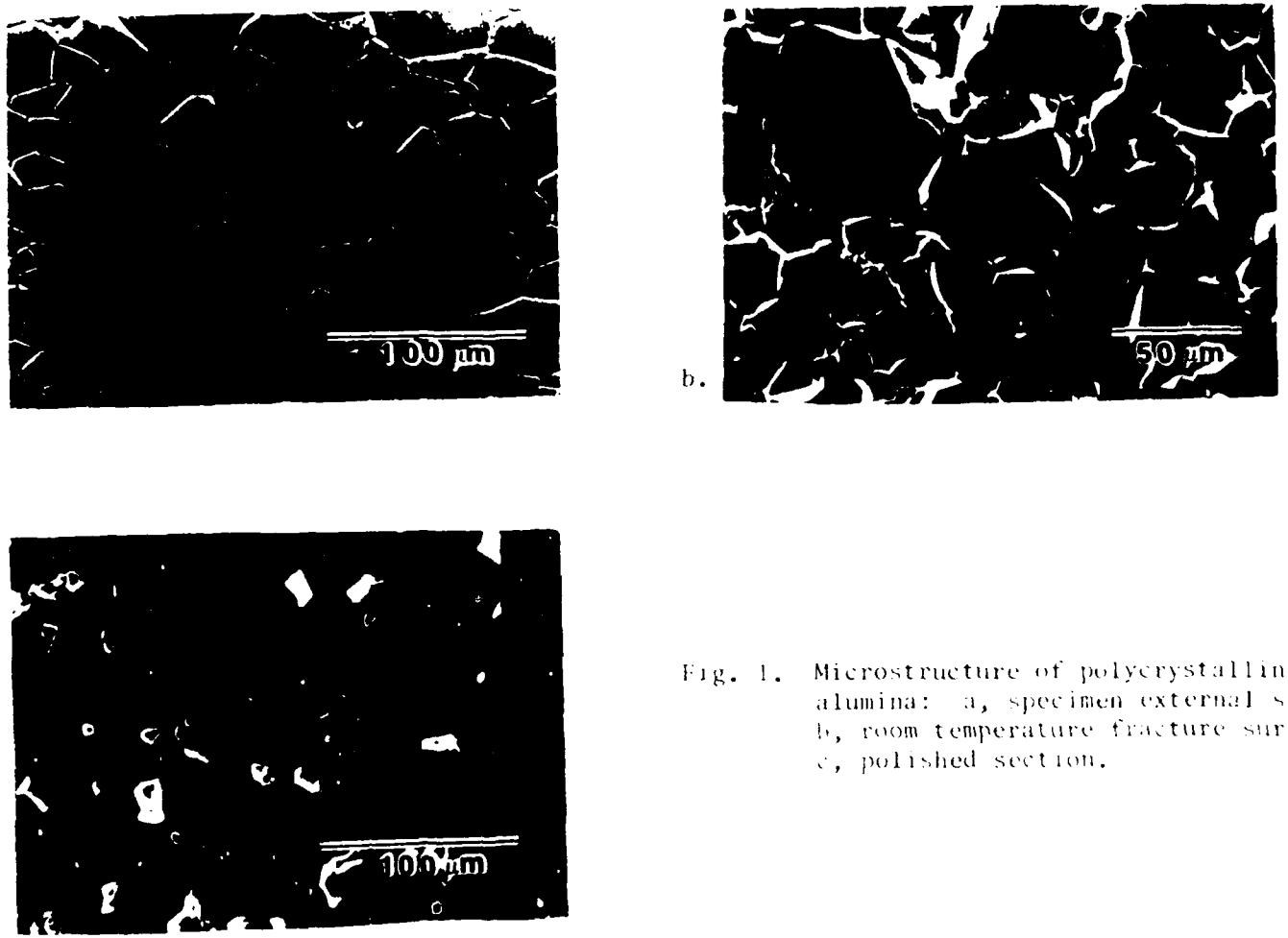

Fig. 1. Microstructure of polycrystalline alumina: a, specimen external surface; b, room temperature fracture surface and c, polished section.

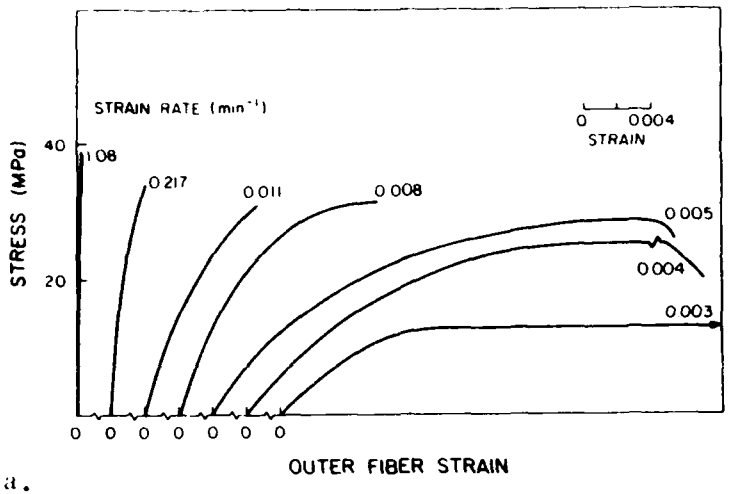

a.

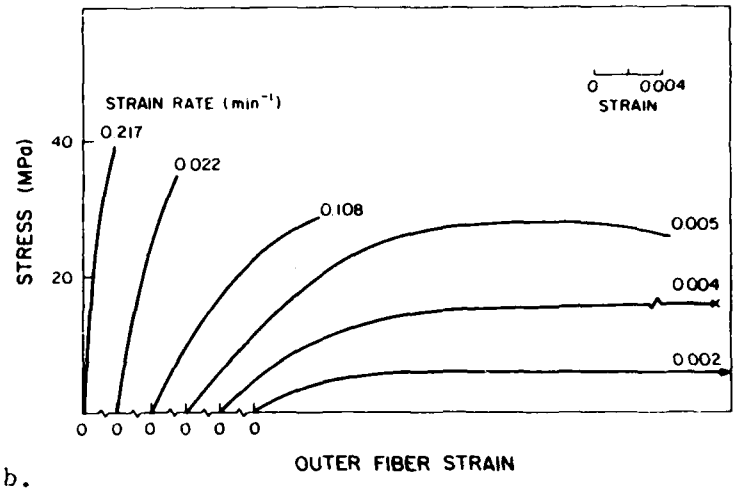

b.

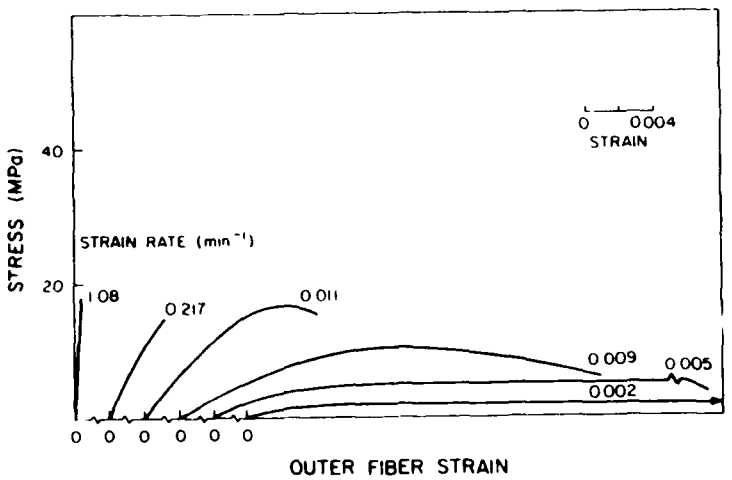

c.

Fig. 2. Stress-strain behavior of polycrystalline alumina at: a, 1650; b, 1700 and c, 1750°C.

Fig. 3. Tensile surface of polycrystalline alumina deformed at a creep rate of 0.0011 min^{-1} at 1650°C.

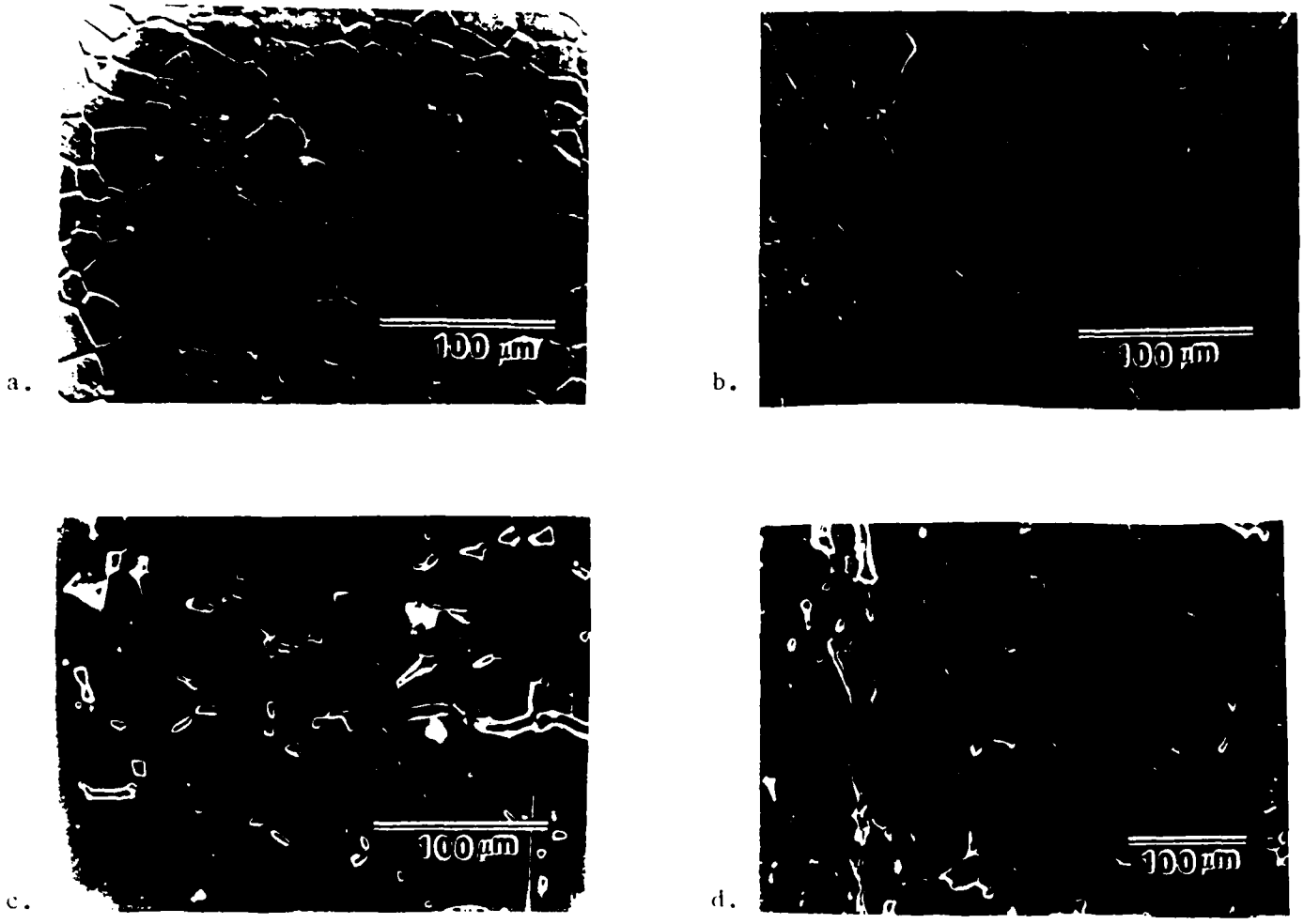

Fig. 4. Microstructures of polycrystalline aluminum oxide deformed at 1650°C and 0.0033 min^{-1}: a, surface subjected to tension; b, surface subjected to compression; c, section subjected to tension and d, section subjected to compression.

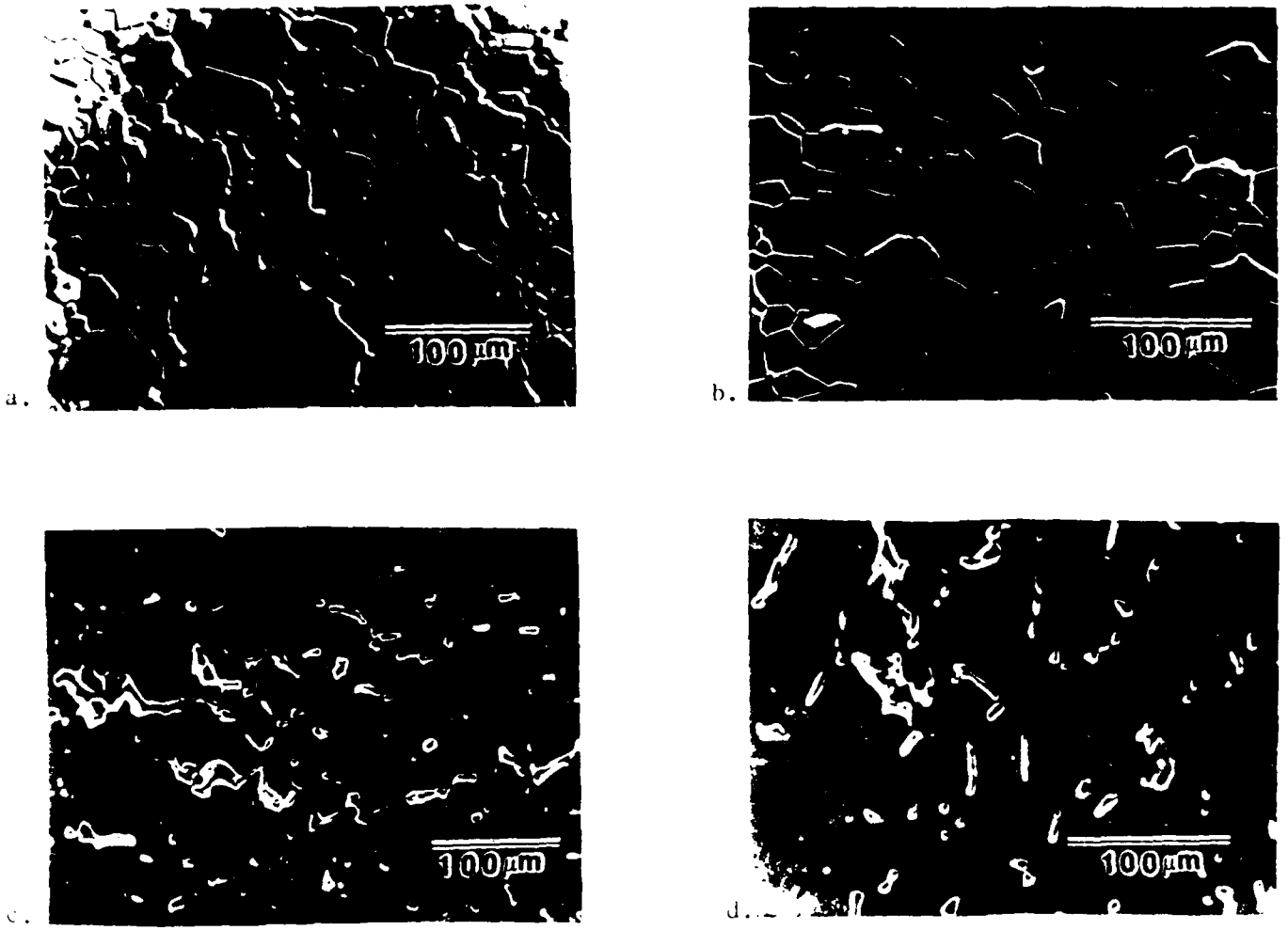

Fig. 5. Microstructures of polycrystalline aluminum oxide deformed at 1650°C and 0.0043 min^{-1}: a, surface subjected to tension; b, surface subjected to compression; c, section subjected to tension and d, section subjected to compression.

Fig. 6. Scanning-electron micrographs of polycrystalline alumina deformed at $0.0054\ min^{-1}$ and $1650^{o}C$: a, tensile surface; b, compressive surface.

Fig. 7. Tensile surface of polycrystalline alumina deformed at 0.0108 min^{-1} and 1650°C.

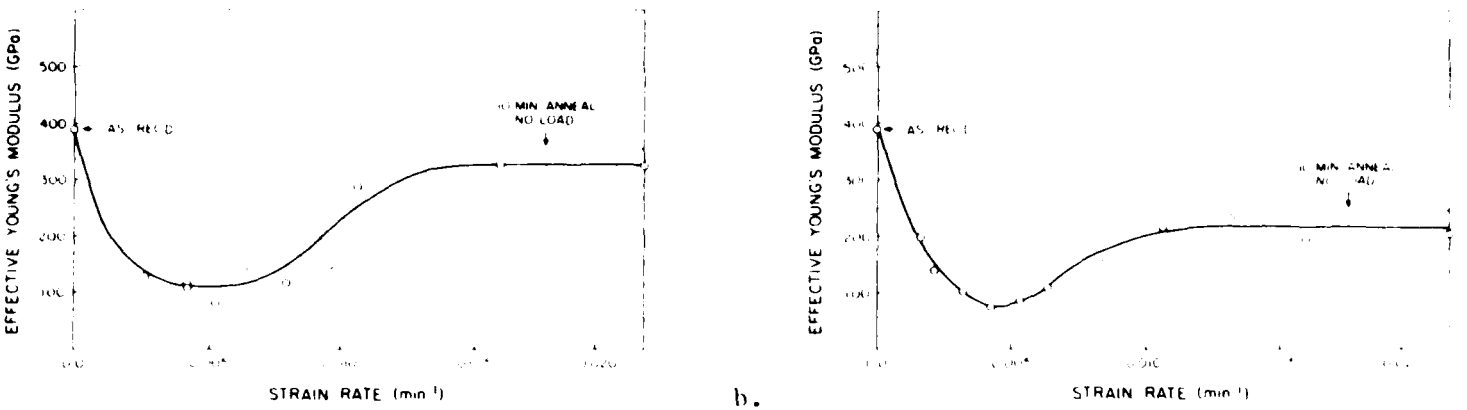

Fig. 8 Effective Young's modulus of polycrystalline alumina deformed to approx. 75% of failure strain as a function of strain-rates at: a, 1650 and b, 1700°C.

Fig. 9 Microstructures of polycrystalline aluminum oxide deformed to approx. 75% of failure strain at 1650°C and 0.0043 min^{-1} for measurement of effective Young's modulus: a, surface and b, section subjected to tension.

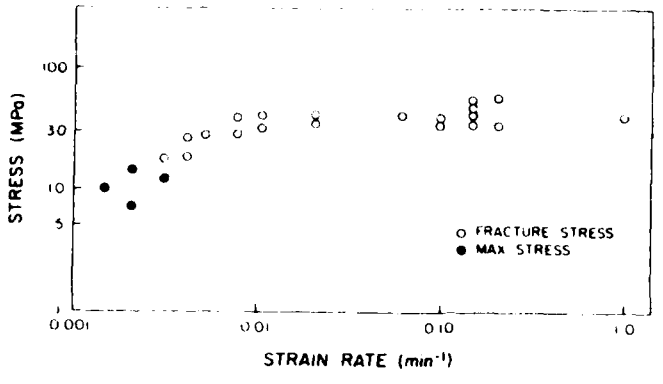

a.

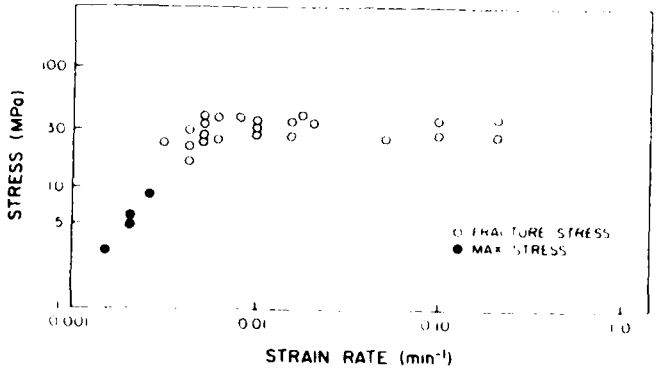

b.

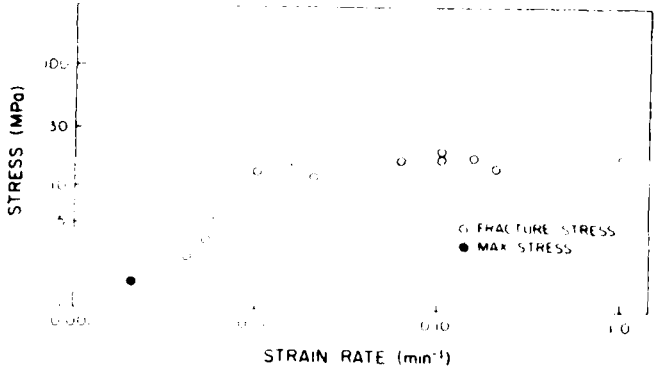

c.

Fig. 10. Strain-rate sensitivity of the failure stress of polycrystalline alumina fractured at: a, 1650; b, 1700 and c, 1750°C.

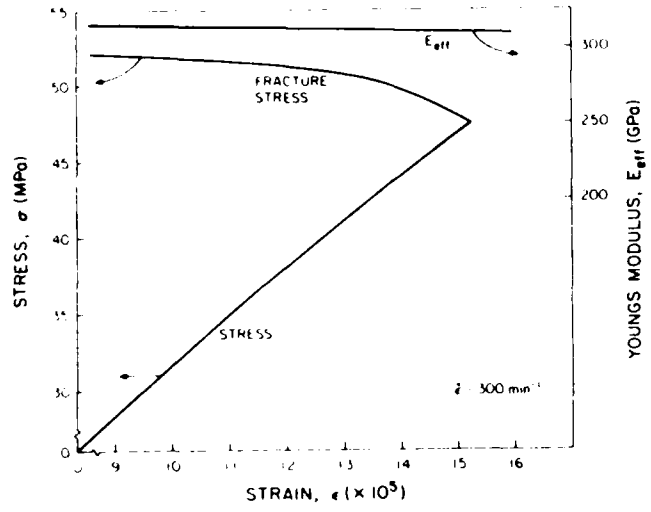

a.

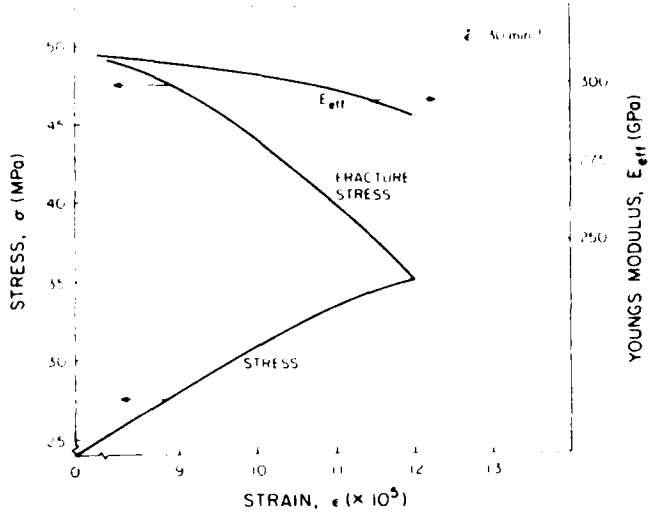

b.

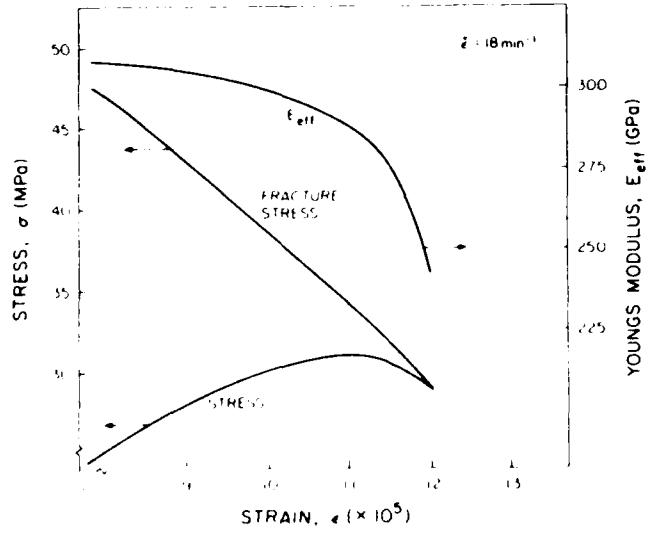

c.

Fig. 11. Calculated dependence of stress, fracture stress and effective Young's modulus on strain for polycrystalline alumina undergoing sub-critical crack growth and diffusional creep strain rates of: a, 300; b, 30 and c, 18 min.$^{-1}$ at 1700°C (Cont'd on next page).

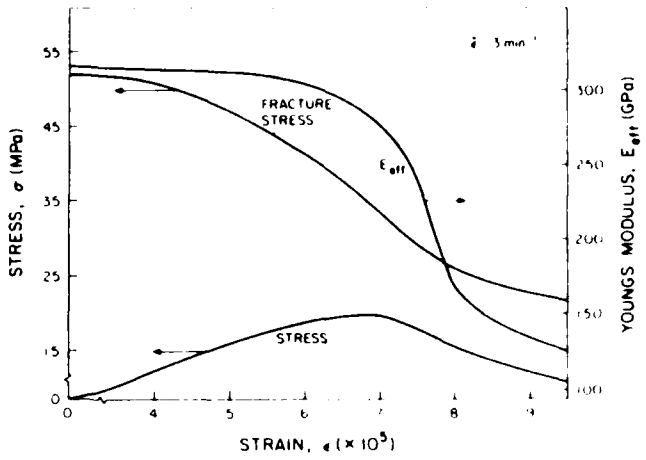

d.

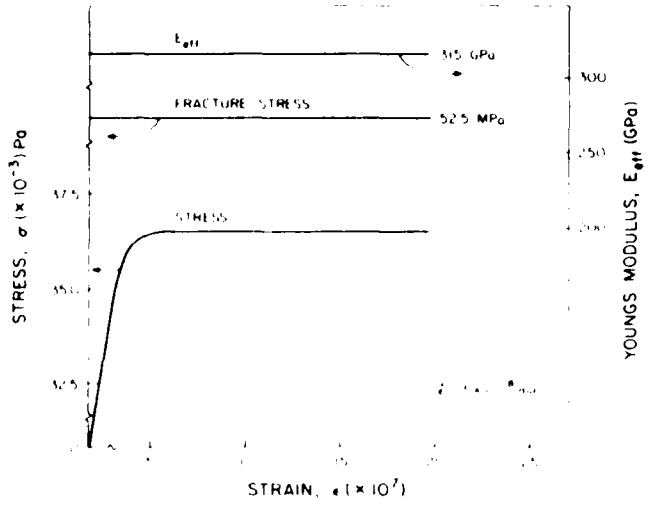

e.

Fig. 11. cont'd. Calculated dependence of stress, fracture stress and effective Young's modulus on strain for polycrystalline alumina undergoing sub-critical crack growth and diffusional creep at strain rates of: d, 3 and e, 3×10^{-8} min^{-1} at 1700°C.

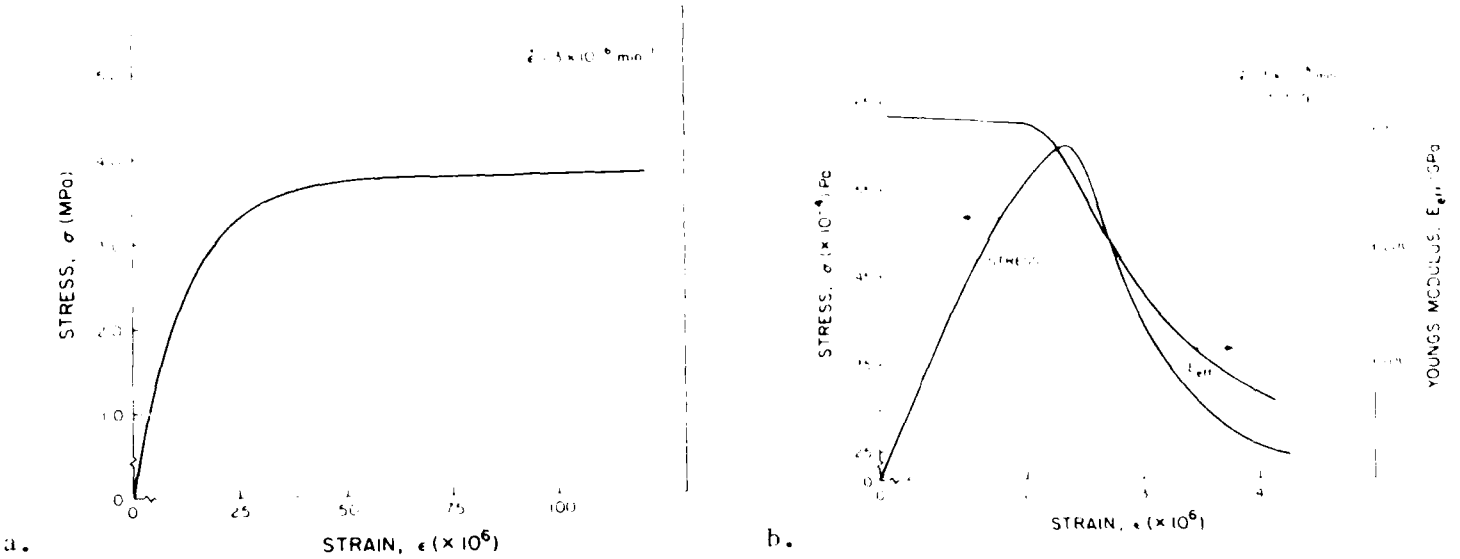

Fig. 12. Calculated stress-strain response of polycrystalline alumina subjected to mechanical loading at a strain-rate of 3×10^{-6} min^{-1} at $1700^{o}C$ undergoing diffusional creep: a, without and b, with sub-critical crack formation and accompanying decrease in effective Young's modulus.

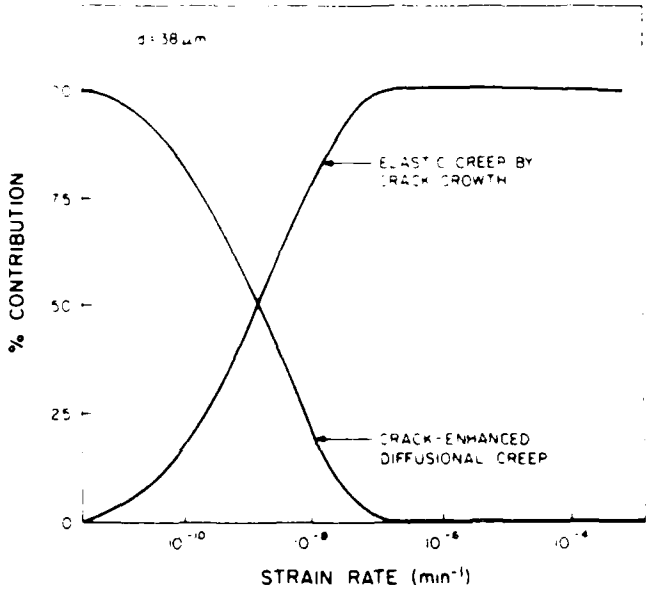

Fig. 13. Calculated relative contributions of Nabarro-Herring diffusional creep and creep by sub-critical crack formation to non-linear deformation of polycrystalline aluminum oxide at 1700°C as a function of strain rate for a grain size of 38μm.

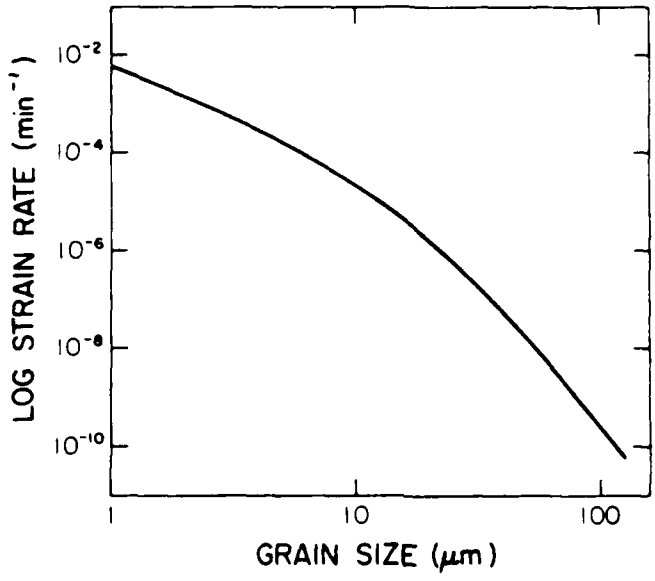

Fig. 14. Grain size dependence of creep rate at which diffusional and elastic creep by crack growth make equal contributions.

END

DATE

FILMED

5-88

DTIC